

**Post-tectonic landscape evolution in NE Iberia using staircase terraces:  
combined effects of uplift and climate**

Claudia J. Lewis<sup>1</sup>, Carlos Sancho<sup>2\*</sup>, Eric V. McDonald<sup>3</sup>, José Luis Peña-Monné<sup>4</sup>, Emilio L.  
Pueyo<sup>5,6</sup>, Edward Rhodes<sup>7</sup>, Mikel Calle<sup>8</sup>, Ruth Soto<sup>5,6</sup>

<sup>1</sup> Earth and Environmental Sciences Division, Los Alamos National Laboratory, 87545  
Los Alamos, NM, USA

<sup>2</sup> Ciencias de la Tierra, Universidad de Zaragoza, Pedro Cerbuna 12, 50009 Zaragoza,  
Spain

<sup>3</sup> Desert Research Institute, 2215 Raggio Parkway, Reno, NV, USA

<sup>4</sup> Geografía y Ordenación del Territorio, Universidad de Zaragoza, Pedro Cerbuna 12,  
50009 Zaragoza, Spain

<sup>5</sup> Instituto Geológico y Minero de España, Unidad de Zaragoza, Manuel Lasala 44,  
50006 Zaragoza, Spain

<sup>6</sup> Unidad Asociada en Ciencias de la Tierra IGME-Universidad de Zaragoza

<sup>7</sup> Department of Geography, The University of Sheffield, Sheffield S10 2TN, UK

<sup>8</sup> Museo Nacional de Ciencias Naturales, CSIC, José Gutiérrez Abascal 2, 28006 Madrid,  
Spain

**\* Corresponding author:**

60  
61  
62 19 Carlos Sancho Marcén  
63  
64 20 Departamento de Ciencias de la Tierra  
65  
66  
67 21 Universidad de Zaragoza  
68  
69 22 Pedro Cerbuna, 12  
70  
71 23 50009 Zaragoza  
72  
73 24 Spain  
74  
75  
76 25 Email: csancho@unizar.es  
77  
78 26 Phone: +34976761091  
79  
80  
81 27  
82  
83  
84  
85 28  
86  
87  
88 29  
89  
90  
91 30  
92  
93  
94  
95 31  
96  
97  
98 32  
99  
100  
101 33  
102  
103  
104  
105 34  
106  
107  
108 35  
109  
110  
111 36  
112  
113  
114  
115 37  
116  
117  
118

## Abstract

River incision into bedrock resulting from the combined effects of tectonic uplift and climate governs long-term regional landscape evolution. We determined spatial and temporal patterns of post-orogenic stream incision from a sequence of well-preserved staircase terraces developed over the last 1 Ma in the Central Pyrenees and its southern foreland Ebro basin (NE Spain). Extensive remnants of ten vertically separated terraces (Qt1 to Qt10, from oldest to youngest) were mapped along 170 km of the Cinca River valley, transverse to the Pyrenean mountain belt. Multiple outcrops appear in the upper reach of the valley (Ainsa sector, 50 km from headwaters) as well as in the lower reach (Albalate sector, 125 km from headwaters). Fluvial incision into bedrock was calculated using (i) differentially corrected GPS measurements of the altitude of straths and (ii) numerical dating of alluvial sediments from the lower terraces (Qt5 to Qt9) by Optically Stimulated Luminescence, previously reported by Lewis et al. (2009), and supplemented with new dates for the upper terraces (Qt1, Qt2 and Qt3) based on palaeomagnetism and supported by soil development. Considering altitude differences and the elapsed time between successive well preserved terrace couples (Qt3-Qt7, Qt7-Qt9 and Qt9-Active channel), mean bedrock incision rates ranged from 0.76 to 0.38 m ka<sup>-1</sup>, at the upper reach of the valley (Ainsa section), and from 0.61 to 0.20 m ka<sup>-1</sup>, at the lower reach (Albalate section). River incision along the valley produced vertically separated, near-parallel longitudinal terrace profiles evidencing a rapid near-uniform regional uplift as response to (i) the tectonic lithospheric thickening in NE Iberia and (ii) the erosional download rebound related to the Ebro basin exorheism. Moreover, a subtle upstream divergence of strath profiles

may have been a consequence of an increase in uplift rate toward the head of the valley. Additionally, incision rates changed over time as indicated by results from the lower reach (Albalade section); the maximum rate was  $1.48 \text{ m ka}^{-1}$  between Qt7 (61 ka) and Qt8 (47 ka), and the minimum rate was  $0.11 \text{ m ka}^{-1}$  between Qt3 (401 ka) and Qt5 (178 ka). The highest incision rates were produced after the Marine Isotope Stage 4 most likely in response to (i) an increased snowmelt discharge during the subsequent deglaciation related to the last maximum advance of glaciers in the southern Pyrenees, and (ii) a limited width of the valley after Qt7 formation, resulting from the deactivation of the westward river migration. Therefore, incision rates over the last 1 Ma in the Cinca River valley were basically controlled by near-uniform bedrock uplift, in the context of climate variability. The results reported in this study represent significant data on fluvial incision in NE Iberia, and provide an assessment of the regional post-tectonic landscape evolution.

**Key words:** Fluvial incision, Staircase terraces, Uplift, Climate change, Mid- to Late Pleistocene, Southern Pyrenees and Ebro Basin

## 1. Introduction

Landscape evolution represents a morphotopographic balance resulting from interactive competition between tectonics, climate and denudation processes (e.g., Burbank and Anderson, 2001; Willet et al., 2006; Cloetingh and Willett, 2013). Fluvial terraces are excellent geomorphic markers that have been used extensively to document landscape evolution (e.g., Bridgland and Westaway, 2008; Westaway et al., 2009). Long-term geomorphic configuration of fluvial systems involves the entrenchment of river valleys and the creation of staircase terrace sequences in response to the basic driving forces of regional climate, tectonic uplift and base level (e.g., Bridgland, 2000; Starkel, 2003; Gibbard and Lewin, 2009; Westaway et al., 2009; Stokes et al., 2012; Pazzaglia, 2013; Wang et al., 2015).

Terraces as geomorphic markers to assess fluvial incision and landscape development have been commonly used worldwide under different orogenic and post-orogenic geodynamic contexts. At a regional scale, deciphering the nature and history of fluvial incision in the Iberian Peninsula, which has an extensive network of terraces, has been limited and remains an unsolved challenge. Undoubtedly, the general lack of well chronologically referenced terrace systems (Santisteban and Schulte, 2007) is determinant. Several regional studies on river incision have been reported by Cunha et al. (2005, 2008, 2012) and Martins et al. (2009, 2010) in the Portuguese reach of the Tagus River, Antón et al. (2012) and Silva et al. (2013, 2016) in the Spanish reaches of the Duero and Tagus rivers, Stange et al. (2013; 2016) in the Segre River valley in the southern Pyrenees, Soria-Jáuregui et al. (2016) in the upper sector of the Ebro River valley, Scotti et al. (2014) and Giacheta et al. (2015) in the Iberian Ranges (NE Spain),

and Viveen et al. (2014) in the Miño River basin from northwest Iberian. Additionally, data on regional fluvial incision need to be integrated within the geodynamic models explaining the Iberian topography and with the regional Pleistocene climate reconstruction for southwestern Europe.

The Spanish Pyrenees and the adjacent Ebro foreland basin comprise an outstanding area to deduce post-orogenic river incision rates and landscape development from staircase terraces and to discuss the uplift mechanisms and the climate changes involved. In this paper we use a well characterized sequence of staircase terraces located along the Cinca River valley, one of the most important Pyrenean tributaries of the Ebro River in northeast Iberia, to evaluate post-tectonic landscape evolution. Reported results are based in a combination of (i) reconstructed longitudinal strath profiles starting from previously mapped terraces (Sancho, 1988), (ii) numerical ages using optically stimulated luminescence (OSL) and supported by time-related trends in soil development (Lewis et al., 2009), and (iii) new palaeomagnetic and soil stratigraphic data. We use our results to deduce spatial and temporal patterns in river incision rates and to discuss the combined action of uplifting and climate change governing the formation of staircase terrace sequences in NE Iberia.

## **2. Study area**

### **2.1 The Cinca River valley**

The Cinca River valley straddles the south-central Pyrenees and the northern Ebro basin (NE Spain) (Figs. 1, 2A). Mean annual precipitation varies from > 2,000 mm in the high Pyrenees to < 400 mm in the semiarid Ebro basin. The Cinca River is 170 km long;

it has a drainage area of 9,700 km<sup>2</sup> and a mean annual flood discharge of 79 m<sup>3</sup>/s. The natural fluvial regime of the Cinca River is altered by the presence of two large reservoirs: the El Grado and Mediano dams (Fig. 3A).

The headwaters area of the Cinca River is glaciated and is located in the Pyrenean Internal Sierras (Monte Perdido summit: 3,355 m a.s.l.). The Cinca River drains to the south and is perpendicular to the Pyrenean belt, joining the larger and eastward-flowing Ebro River in the Ribarroja reservoir (90 m a.s.l.) in the central Ebro Basin. This river confluence is more than 100 km up gradient from the Mediterranean Sea (Fig. 1). The Cinca River in the upper valley (from headwaters to Ainsa; Figs. 1, 3A) is a mixed bedrock-alluvial channel, whereas the Cinca River in the lower valley (from Basbastro to the mouth into the Ebro River; Figs. 1, 3A) is an alluvial gravel channel. Several slight knickpoints can be identified along the active channel profile: however, only the knickpoint located at El Grado (External Pyrenees) is noticeable (Figs. 2B, 3A).

## **2.2 Geologic setting**

Geologically, the Cinca River valley is excavated in the Pyrenean belt and the adjacent Ebro foreland basin (Fig. 2A). The Pyrenees constitutes a WNW-ESE striking, narrow asymmetric alpine chain with a mainly southward vergence, developed from the Late Cretaceous to the Early Miocene. This structural setting was formed in response to the partial subduction of the Iberian lithosphere underneath Europe (e.g., Muñoz, 2002). The southern central Pyrenees comprise part of the Axial Zone, formed by a basement and a series of imbricated thrust sheets, involving Mesozoic to Eocene cover rocks and affecting synorogenic Tertiary materials (e.g., Martínez-Peña and Casas-Sainz, 2003).

Specifically, the Cinca River valley is located at the western border of the South Pyrenean Central Unit that is characterized by north-south oblique structures that control the north-south alignment of the Cinca River (Martínez-Peña et al., 1995). From a stratigraphic point of view, the Cinca River traverses the western sector of the Graus-Tremp basin (the Ainsa sub-basin) (Fig. 2B), a piggy-back basin filled with Palaeocene-Eocene deposits (Puigdefábregas and Souquet, 1986).

The Tertiary Ebro basin was formed during the Palaeogene as a consequence of flexural subsidence related to growth of the surrounding mountain chains, particularly the Pyrenees. Sedimentation into the closed basin continued under conditions of continental internal drainage during Oligocene and Miocene times (Muñoz et al., 2002; Costa et al., 2010) (Fig. 2B). This sedimentary regime persisted until the end of the late Miocene (between 12.5 and 8.5 Ma) when the internal drainage of the Ebro basin ended due to aggradation of the lacustrine system and extensional geodynamic conditions in the western Mediterranean basin (García-Castellanos et al., 2003). The Ebro basin was subsequently opened when headward erosion of coastal drainage captured the internally draining system. The Ebro sedimentary basin was then incised and previous depositional units were excavated and transported to the coastal Mediterranean.

Erosional activity of the drainage in the Pyrenees and the Ebro Basin persisted throughout the Quaternary. Subsequent fluvial activity developed extensive staircase terrace sequences along the Ebro drainage system (e.g., Gutiérrez and Peña, 1994; Peña, 1994). The earliest evidence of alluviation in the exoreic Ebro basin is at ca. 1.28



Ma in the Alcanadre River valley, a tributary of the Cinca River (Duval et al. 2015; Sancho et al., 2016).

### ***2.3 Approach to the Cinca River terrace sequence***

Two basic configurations of stream terraces, strath and fill terraces, are commonly differentiated, based on the morphology of the erosional surface and thickness of alluvial sediments (Bull, 1991; Pazzaglia, 2013). A strath terrace is characterized by a subhorizontal erosional surface carved into bedrock mantled with a thin mobile alluvial cover of a bedrock channel that does not exceed the depth of scour of the stream. In contrast, fill terraces are characterized by an irregular basal surface covered by a layer of thick alluvium that accumulates when the channel vertically exceeds the depth of scour, during periods of valley aggradation (Wegmann and Pazzaglia, 2009; Pazzaglia, 2013). The thickness of the alluvial cover is a long-discussed criterion to distinguish between both types of terrace (Pazzaglia, 2013). Mobile alluvial cover associated with strath terraces rarely exceeds 5 m in thickness even for large watersheds, while greater alluvial thickness is usually related to fill terraces (Pazzaglia, 2013).

The studied terrace sequence in the Cinca River valley consists of 10 extensive paired cyclic stream terraces (Sancho, 1988; Lewis et al., 2009). The mean thickness of the alluvial mantle covering the straths is around 5 m, ranging from 8 m for the oldest terraces to 3 m for the youngest terraces. The general morphology of strath surfaces is broadly subhorizontal. Given this description, the Cinca River terrace sequence is closer to a strath relative to a fill terrace and displays a strath-like terrace. We

recognize that in places, a near-fill terrace configuration related to slight valley aggradations could be considered.

### 3. Methods: using terrace straths to measure river incision

Determination of the river incision rate (e.g., Burbank and Anderson, 2001) for a point along a river valley is given by the ratio between the height (m) of the terrace strath above the active channel and the timing (ka) of terrace formation. We expanded this approach to calculate the river incision rate between a given pair of terraces; the fluvial incision rate ( $I_{Q_{ti}-Q_{tj}}$ ) (m/ka) between any two terraces  $Q_{ti}$  and  $Q_{tj}$ , is given by the relation:

$$I_{Q_{ti}-Q_{tj}} = H_{Q_{ti}-Q_{tj}} / T_{Q_{ti}-Q_{tj}}$$

where  $H_{Q_{ti}-Q_{tj}}$  is the difference of altitude (m) of the terrace straths  $Q_{ti}$  and  $Q_{tj}$ , and  $T_{Q_{ti}-Q_{tj}}$  is the elapsed time (ka) between them.

We use the terrace straths rather than the terrace treads to measure river incision rates (Wegmann and Pazzaglia, 2009) because tread surfaces can be subsequently modified through both aggradation or degradation. Observations of terrace stratigraphy indicate that in places the terrace surface has been aggraded through deposition of lateral alluvial and aeolian sediments or degraded through erosion removal and lowering of the original terrace surface as indicated by severely truncated or missing soil profiles.

#### 3.1 Height of terrace straths and the active channel

Collecting and assessing height measurements of bedrock strath surfaces requires compiling a detailed regional geomorphological framework. Geomorphic mapping was undertaken on an aerial photographic base (1:18,000 in scale) and was extensively field checked along the Cinca River valley. Ten terraces were firstly identified (Qt1 to Qt10, from higher to lower) from their altitudinal position (Sancho, 1988; Lewis et al., 2009). Correlation of terraces was primarily based on geomorphologic and stratigraphic relationships between terraces and was reinforced with soil development and numerical dating. Elevations of the differentiated strath terrace surfaces and the Cinca active channel were measured to sub-meter accuracy using a global positioning system (GPS) differentially corrected to a permanent base station. Measurements were occasionally supplemented by data from 1:25,000-scale topographic maps. Height measurements allowed reconstruction of accurate profiles of strath terraces and the active channel.

### ***3.2 Chronology of terraces***

Timing of strath preservation is broadly based on the basal age of overlying fluvial deposits. We used numerical dates previously provided by Lewis et al. (2009), based on OSL of quartz grains dating and supported by soil stratigraphy. These data are available only for the lower terraces (from Qt5 to Qt9) corresponding to both the Penultimate and the Last Glacial cycles. In this study we provide new chronological evidence for the older terraces using paleomagnetic analysis and time-related trends in soil development.

#### ***3.2.1 Paleomagnetic sampling and laboratory procedures***

Characterization of the paleomagnetic polarity has been a powerful tool for unravelling terrace ages since the pioneering work of Pevzner (1970). Subsequent applications have focused on locating the Brunhes/Matuyama (B/M) boundary (Dubar and Semah, 1986; Jacobson et al., 1988) or even shorter polarity events within the Brunhes and Matuyama periods (Li et al., 1997). Paleomagnetic analysis was conducted on the Cinca River alluvium overlying the strath terraces to identify the location of the B/M boundary. Previous results in the Central Ebro Basin (Gil et al., 2013) and in the Alcanadre River (tributary of the Cinca River; Calle et al., 2015; Sancho et al., 2016) allowed us to be confident of the suitability of the method provided that an adequate sampling was guaranteed (Gil Garbi, 2017).

Sampling for paleomagnetic analysis was performed in 13 pits excavated in the upper terraces along the valley (from Qt1 to Qt7). Siltstone layers within alluvial sequences were the main targets to ensure a stable paleomagnetic signal. Sampling tools designed for unconsolidated sediments were used instead standard drilling machines. Subsequent consolidating techniques using non-magnetic chemical compounds (sodium silicate and alumina cement) were used to obtain standard and stable paleomagnetic specimens (Pueyo et al., 2006). Oriented blocks were occasionally sampled.

Present-day declination ( ~ 1° 30'W) during the sampling was corrected in the core orientations (NOAA's National Geophysical Data Center, <https://www.ngdc.noaa.gov/>). Stepwise and detailed demagnetisation (both thermal [TH] and alternating field [AF]) was conducted in the paleomagnetic laboratory at the University of New Mexico (UNM) (Albuquerque) and at the Institute of Earth Sciences "Jaume Almera" (Consejo

Superior de Investigaciones Científicas-Universitat de Barcelona). TH demagnetisation was run with a TSD-1 furnace (Shonsted Ltd.), and remanent magnetization was measured with a 2G three-axis SQUID magnetometer in both laboratories. The 2G-AF demagnetizer was only used in the UNM laboratory.

Thermal stepwise demagnetisation used intervals of 50°C between room temperature and 550-600°C and AF increments between 3 and 10 mT up to 100mT (following an exponential trend) were run to characterize all paleomagnetic components of the NRM. Paleomagnetic directions were fitted by principal components analysis (PCA; Kirschvink, 1980) using the Paldir software by Utrecht Universiteit. In some cases, demagnetization circles (Bailey and Halls, 1978), the stacking routine (Scheepers and Zijdeveld, 1992) and the virtual directions method (Ramón and Pueyo, 2017) were used to double-check the PCA results. Site means and terrace means were fitted by Fisher (1953) statistics. It is a probability distribution for multivariate directional data (vectors or simple lines in the 3D space).

### *3.2.3 Soil development*

Soil development indices were used locally and regionally to correlate principal terrace levels (Lewis et al., 2009) and to estimate the age of the Qt3 terrace. Soils were described according to standard methods and nomenclature of the U.S. Soil Survey Staff (1993). Carbonate stage morphology follows nomenclature of Gile et al. (1981) and Birkeland (1999). Time-related changes in soil morphology were analyzed using a well-tested soil development index (SDI) (Harden, 1982; Harden and Taylor, 1983; McDonald et al., 1996) based on a soil chronofunction presented in Lewis et al. (2009).

SDI values were calculated using a conversion of soil morphologic properties (rubification, texture, structure, dry consistence, moist consistence, secondary carbonates, lightening, and argillans) into numerical data to enable a quantitative comparison of the degree of soil development. Horizon Development Index (HDI) values are obtained by normalizing each set of properties and a Profile Development Index (PDI) is calculated from HDI values and horizon thickness. The PDI values reflect the overall degree of soil development and provide a means of comparison among soils within a given sequence or area. The PDI has proven useful for providing correlations and calibrated age estimates for the sequence of strath terraces from the Cinca River valley (Lewis et al., 2009).

## 4. Results

### *4.1 Morphopedosedimentary characteristics of the staircase terrace sequence*

The marked vertical separation between adjacent terraces, reinforced with extensive outcrops and their longitudinal continuity, facilitated mapping, regional correlation of terrace remnants, and descriptions of the fluvial terrace deposits along 170 km in the Cinca River valley (Figs. 3, 4). Ten paired staircase terraces (numbered Qt1, Qt2, Qt3, Qt4, Qt5, Qt6, Qt7, Qt8, Qt9, and Qt10, from oldest to youngest) have been preserved (Appendix 1). The terrace development and preservation are prominently displayed in the upper reach of the valley (near Ainsa, 50 km from the headwaters) and immediately downstream of the confluence with the Ara River (Figs. 3B, 4A, D). Mean height of the terrace straths above the active channel of the Cinca River in this sector are 172.5 m (Qt3), 44.2 m (Qt7) and 6.0 m (Qt9) (Table 1). The corresponding vertical

separations between adjacent preserved strath terraces are 128.3 m (Qt3-Qt7) and 38.2 m (Qt7-Qt9) respectively.

The lower reach of the valley goes from the External Pyrenees, where the Cinca River enters into the Ebro Basin, to the confluence with the Ebro River, including several important tributary junctions (the Esera, Vero and Alcanadre rivers). The lower reach shows the widest and best preserved terraces (Fig. 4B, E, F), particularly in the Albalate-Belver sector (125 km from the headwaters; Fig. 3C). Mean height of the terrace straths above the active channel of the Cinca River in this sector are 182.1 m (Qt1), 132.5 m (Qt2), 103.5 m (Qt3), 91.3 m (Qt4), 79.9 m (Qt5), 60.4 m (Qt6), 33.9 m (Qt7), 13.1 m (Qt8) and 3.6 m (Qt9) (Table 1). The corresponding vertical separations between adjacent strath terraces are 49.6 m (Qt1-Qt2), 29.0 m (Qt2-Qt3), 12.2 m (Qt3-Qt4), 11.4 m (Qt4-Qt5), 19.5 m (Qt5-Qt6), 26.5 m (Qt6-Qt7), 20.8 m (Qt7-Qt8) and 9.5 m (Qt8-Qt9).

Terraces Qt3, Qt7 and Qt9 are broadly preserved along the Cinca River valley (Appendix 1). Terraces older than Qt7 are preserved only on the river's east bank, indicating the westward migration of the Cinca River. This migration is well noted in the Albalate-Belver sector and reaches a lateral westward displacement of 8 km between Qt1 at Monte Julia and Qt7 at Albalate (Fig. 3C). Qt7 and subsequent Qt8 and Qt9 terraces outcrop in both sides of the valley. This implies a significant change in the width of the valley. In fact, Qt7 is approximately 5 km wide in the Albalate-Alcolea section, whereas the current valley bottom (active channel and floodplain) reaches a maximum width of 2 km (Fig. 3C).

Terrace treads are typically broad (2-4 km width) and commonly underlain by 2.8-7.7 m (Fig. 4C) of largely cobble-rich gravel with a sand-rich matrix, large (20-100 cm diameter) sub-rounded boulders, sparsely populated with sand lenses, and capped by either gravelly sand-rich alluvium or finer-textured overbank deposits. Fluvial deposits occur in fining-upwards sequences. According to lithofacies of Miall (1978), gravels are generally massive but locally imbricated (Gm) and cross-stratified (Gt, Gp), are well-sorted and sub-rounded and consist of limestone, sandstone, granite, quartzite, and schist (in order of decreasing abundance) of Pyrenean and, locally, Ebro basin provenances. Interbedded sand lenses can be cross-stratified (St, Sp) or horizontally laminated (Sh). Gravels can be capped by overbank silts (Fm).

Strath surfaces are carved into Cretaceous to Eocene marine carbonates and marls (Fig. 4A) along the river's Pyrenean reach and Eocene-Miocene continental deposits (Fig. 4B) along the Ebro Basin reach (Fig. 2B; Appendices 1 and 2). Localized deformation of the strath surface and associated gravels (e.g., tilting and faulting) occurs in places and is related to salt diapirism and gypsum dissolution confined to the Barbastro anticline and the Estada-Estadilla diapir (Sancho, 1988, 1989; Lucha et al., 2008) (Appendix 1). Local deformation related to small vertical faults was also observed near El Grado and El Pueyo de Araguás.

The Qt1 terrace is poorly preserved and only occurs between Albalate and Binaced (Figs. 3C, 4F; Appendix 1), where remnants occur as isolated hills (San Salvador and Las Brujas sites). The Qt1 remnants constitute the highest preserved remnants of the Cinca River terrace sequence. Mean thickness of alluvial cover is around 7.7 m and maximum grain size (Dmax) ranges from 30-48 cm (mean value  $42\pm9$  cm) (Appendix 2). An



eroded petrocalcic soil horizon ( ~1 m thick) formed in fine-grained sediments is preserved in places.

The Qt2 strath terrace is more or less continuously preserved between Albalate and Belver and is in the vicinity of the Qt1 remnants (Figs. 3C; Appendix 1). Mean thickness of alluvial cover preserved is around 5.6 m and maximum grain size (Dmax) ranges from 36-48 cm (mean value  $41\pm4$  cm) (Appendix 2). The soils found on the Qt2 are only weakly to moderately developed and are considerably less developed than the soils on the younger Qt3 terrace. This indicates that the original terrace surface has been severely eroded.

The Qt3 terrace is one of the two most important geomorphic features along the Cinca River valley. It is preserved continuously in the lower reach of the valley between Monzón and Fraga (Figs. 3C, 4F; Appendix 1); other relevant outcrops have been identified at Barbastro, El Grado and Ainsa (Figs. 3B, 4D; Appendix 1). Mean thickness of alluvial cover is around 5.8 m and maximum grain size (Dmax) ranges from 26-50 cm (mean value  $34\pm6$  cm) (Fig. 5; Appendix 2). Locally the Qt3 deposit near El Grado is faulted. Soil characteristics on this terrace are described below.

The Qt4 terrace is preserved only between Barbastro and Fraga (Figs. 3C, 4E; Appendix 1). Mean thickness of alluvial cover is around 5.2 m and maximum grain size (Dmax) ranges from 26-43 cm (mean value  $35\pm8$  cm) (Appendix 2). Near Belver, the terrace deposits include a 90 cm-thick aeolian cap that overlies 90 cm of overbank fines. An OSL date on the loess cap constrains its age to be  $20\pm3$  ka (Lewis et al., 2009), likely deposited during the MIS2 glaciation. No soils were described on the Qt4 terrace due

to surface erosion. In some localities, reworking of the Qt4 surface is evidenced by a cap of colluvium incorporating pieces of underlying petrocalcic horizons.

The Qt5 terrace is also preserved only between Monzón and Fraga Fraga (Fig. 3C; Appendix 1). Stratigraphic relations between the Qt4 and Qt5 terraces indicate that formation of the Qt5 terrace cannibalized much of the older Qt4 terrace. Mean thickness of alluvial cover is around 4.5 m and maximum grain size ( $D_{max}$ ) ranges from 28-51 cm (mean value  $38 \pm 7$  cm) (Appendix 2). North of Castejón del Puente, the Qt5 terrace was deformed by the diapiric activity of the Barbastro salt anticline (Sancho, 1989). The Qt5 soils in the Albalate sector have well developed Bk and Bkm horizons with stage III+ to IV+ carbonate morphology (Table 2) (Lewis et al., 2009).

The Qt6 terrace is also preserved only between Monzón and Fraga Fraga (Figs. 3C; Appendix 1) and exposures of the deposits are very limited because the degradation of the scarps. Mean thickness of alluvial cover is around 5.1 m and maximum grain size ( $D_{max}$ ) ranges from 24-80 cm (mean value  $39 \pm 19$  cm) (Appendix 2). Soils have a well-developed Btk horizon and stage III+ carbonate morphology (Table 2) (Lewis et al., 2009).

Remnants of the Qt7 terrace occur continuously along approximately 120 km of the Cinca valley (Figs. 3B, C, 4; Appendix 1). This is the best-preserved terrace on the Cinca and the most relevant terrace marker in the landscape. Terrace remnants are broad and up to 4 km in width along the lower reach. Mean thickness of alluvial cover is around 5 m. Maximum grain size ( $D_{max}$ ) ranges from 20-68 cm (mean value  $34 \pm 9$  cm) (Fig. 5; Appendix 2). Local distribution of terraces in the Albalate area suggests that

Qt7 terrace formation cannibalized much of older Qt6 and Qt5 terraces. In some locations, there is 3-4 m of colluvium on top of the Qt7 fluvial deposits. The Qt7 strath surface and overlying deposits are deformed when the underlying bedrock is composed of Upper Triassic evaporites and clays (Estada-Estadilla diapir) and Eocene evaporites (Barbastro salt anticline) (Sancho, 1989; Lucha et al., 2008). Local small faults deform the Qt7 deposits at El Pueyo de Araguás. The Qt7 soils in the Albalate sector have moderately to well-developed Btk horizons and stage II to weak stage III carbonate morphology (Table 2) (Lewis et al., 2009).

The Qt8 terrace is not as extensively preserved as Qt7; it crops out only along the lower 35 km of the valley (Fig. 3C; Appendix 1), where it is 2-3 km wide. Mean thickness of alluvial cover is around 2.7 m and maximum grain size ( $D_{max}$ ) ranges from 22-42 cm (mean value  $29 \pm 6$  cm) (Appendix 2). Soils in the Albalate sector have moderately developed Btk horizons with stage II carbonate morphology (Table 2) (Lewis et al., 2009).

The Qt9 terrace is generally co-extensive with the Qt7 terrace and traceable along 140 km of the total length of the river valley (Figs. 3B, C, 4D, E, F; Appendix 1). The Qt9 terrace is also largely co-extensive with Qt8, where the latter is preserved, and is approximately 2 km wide. Maximum grain size ( $D_{max}$ ) ranges from 12-60 cm (mean value  $29 \pm 12$  cm) (Fig. 5; Appendix 2) and mean thickness of alluvial cover is around 3.3 m. Locally this terrace is considerably thicker (e.g., 10 m at Castejón del Puente) because of deposition across the synsedimentary karstic subsidence on the south flank of the Barbastro salt anticline. The Qt9 soils in the Albalate sector have moderately

developed Bw and Bk horizons with stage I+ carbonate morphology (Table 2) (Lewis et al., 2009).

The Qt10 terrace (Figs. 3B, C, 4E, F), which is in an extensive active floodplain, has Roman bridge abutments preserved on its top near Castejón del Puente, demonstrating that this has been the active surface since at least Roman times in the region (from ca. 140 BC until ca. 400 AD, approximately about 2,000 years ago) (Beltrán, 1985).

#### **4.2 Terrace profiles**

The longitudinal profiles of the terrace straths and the active channel of the Cinca River were reconstructed (Fig. 6) from 300 GPS measurements (Appendices 1 and 2) and a few elevations derived from topographic maps. Strath heights (projected to a common vertical plane down the center of the modern stream valley) reveal several consistent patterns along the length of the Cinca River from headwaters to its confluence with the Ebro River. Several key features of the terrace profiles are significant.

First, the Cinca River has experienced progressive fluvial incision subsequent to formation of the Qt1 terrace, producing a marked vertical separation among terraces (Fig. 6; Table 1). As a consequence, a noticeable and well expressed staircase pattern has developed along the valley.

Second, overall longitudinal profiles are semi-parallel with a slight, but clear, upstream divergence (Fig. 6). The greatest expression of divergence is recorded by the Qt3 terrace with vertical separation between the active channel and strath surface ranging

from 165-175 near Ainsa (km 50), 130-135 m at Barbastro (km 100) and 95-105 m at Zaidín (km 155). Locally variable effects in divergence are observed along the profile due to rock resistance, active faulting, and gypsum diapirism and dissolution; however, these effects cannot explain the first-order longitudinal trends. The Qt7 profile also diverges upstream with respect to the active channel, although not as markedly. For example, the Qt7 is 45-50 m above the active channel near Ainsa, 40 m at Barbastro and 30-35 m near Zaidín.

The log plot of longitudinal profiles also shows changes in gradient at the Pyrenean mountain front. A prominent knickpoint occurs in the active channel at 90 km from the headwaters near El Grado (Fig. 6). This knickpoint is related to the higher erosional resistance of the folded rocks (Cretaceous and Eocene limestones) of the External Pyrenees (Fig. 2B; Appendix 1), as opposed to less resistant clastic sedimentary rocks at the margin of the Ebro basin. The knickpoint appears to be spatially fixed because its location has persisted through time for straths associated with Qt3, Qt7, Qt9 terraces and the active channel.

### **4.3 Terrace chronology**

#### **4.3.1 Geochronology for terraces Qt5 to Qt9**

Numerical ages of the five youngest terraces (Qt5, Qt6, Qt7, Qt8, and Qt9) (Table 3) of the Cinca River sequence have been previously reported by Lewis et al. (2009), from multiple OSL dates and reinforced using regional soil stratigraphy. To summarize, Lewis et al. (2009) obtained two dates for Qt5 terrace ( $171 \pm 22$  ka and  $180 \pm 12$  ka), giving a weighted mean age of  $178 \pm 21$  ka, and one date for Qt6 ( $97 \pm 16$  ka). Six samples from

Qt7 terrace constitute a tightly grouped set of dates ( $63 \pm 12$ ,  $59 \pm 13$ ,  $64 \pm 13$ ,  $61 \pm 3$ ,  $56 \pm 4$  and  $65 \pm 5$ ) with a weighted mean age of  $61 \pm 4$  ka. Five dates on Qt8 terrace ( $39 \pm 5$ ,  $42 \pm 6$ ,  $47 \pm 4$ ,  $50 \pm 4$  and  $50 \pm 3$ ) gave a weighted mean age of  $47 \pm 4$  ka. Finally, eight well grouped OSL dates for Qt9 terrace gave a weighted mean age of  $11 \pm 1$  ka. The Qt7 terrace is correlated with glacial and fluvioglacial deposits in the Cinca headwaters (confluence of the Cinca and Cinqueta rivers at Mesón de Salinas) (Fig. 3A) that have a mean age of  $64 \pm 11$  ka, corresponding to the last maximum glacier extension in the south-central Pyrenees (Sancho et al., 2003). More detailed information from OSL measurements and derivation of mean terrace deposit dates is presented in Lewis et al. (2009).

#### 4.3.2 Paleomagnetic data

The intensity of the NRM from terrace deposits of the Cinca River ranged in intensity from 0.132 to 317 mA/m with an average of 39.98 mA/m ( $\pm 3.8$  mA/m), although 90% of the data were between 0.4 and 200 mA/m (Fig. 7A). After spurious components at very low temperatures (below 200°C), with occasional large intensities, stable paleomagnetic directions were observed between 250 °C and 560-600 °C in the thermal treatment (Fig. 7B). Alternating field treatment was not as successful in isolating stable directions, although some reliable directions (comparable to TH sister samples) were identified from 8-10 mT up to 40 mT (and even 80 mT; see for example samples 77a and 77b) (Fig. 7B). The primary and stable component of the magnetic field is characterized by low-coercivity and medium-temperature minerals pointing to magnetite as the main carrier of the magnetization.

Lower and intermediate terraces (from Qt9 to Qt3) unambiguously registered normal polarity of the primary paleomagnetic field (Fig. 7C). On the other hand, the high level Qt2 terrace unequivocally recorded a reversed polarity. This crucial observation is well supported by the consistent directions obtained in three different pits (T9-1, T9-2 and T9-3) in the Mombrún area (near Albalate) (Table 4). The oldest terrace (Qt1) recorded an intermediate pattern, displaying both polarities and scattered directions, although only one pit was sampled in this terrace. Paleomagnetic directions found in the Cinca terrace sequence, therefore, are consistent (equal demagnetization intervals and carriers), display pseudo-antipodal polarities (N: 355, 58 [ $\alpha_{95}$ : 10.6° and k: 5.7]; R: 220, -48 [ $\alpha_{95}$ : 20.6° and k: 5.74]) and seem to be a reliable record of the primary paleomagnetic field (Fig. 7C).

Despite individual paleomagnetic means that were weakly defined partially due to the small number of demagnetized samples (Table 4), the mean directions and polarities were consistent among the different samples sites across the same terrace. Besides, the stereographic projection merging all data together gives robust and pseudo-antipodal means that allow us to be confident about the primary character of the magnetic record.

In view of these results, a relative chronology can be established (Table 1). All studied terraces younger than Qt3 display a normal polarity and belong to the Brunhes period in agreement with the available OSL dates for Qt5 to Qt9. The Qt2 terrace must belong to the Matuyama reverse period, likely close to the Brunhes/Matuyama reversal, and its boundary (C1r/C1n: 0.773 Ma) (Singer, 2014) must be located between the Qt3 and Qt2 terraces. The poor results found in the Qt1 terrace prevent the proposal of any

reliable interpretation, although they point to the occurrence of another zone with normal polarity. Future chronologic studies may shed light on interpretation and distinguish between Jaramillo and Cobb Mt. normal events. These two hypotheses have been recently proposed in other locations in the Ebro Basin (Sancho et al. 2016; Gil et al., in review).

#### 4.3.4 Qt3 soil characteristics and estimated soil age

Soils formed on the Qt3 surfaces along the upper (Ainsa) and lower (Albalate) reaches of the Cinca River valley have the strongest degree of development relative to soils formed on the younger terraces (Table 2). Soils on the Qt3 terrace near Albalate vary in development, reflecting soils that have formed in either the original cobble-gravel bar deposits or in the original channel settings where the soil parent material consist of fine-textured overbank (with possible aeolian contributions) that overlies gravel-rich alluvium. Soils formed in depositional bars have weakly developed Btk horizons that overlie well-developed Bkm horizons with Stage IV to V carbonate morphology. Soils formed in channel settings have weak- to moderately-developed Btk horizons with stage IV carbonate morphology. Soil depth to the Bkm horizons ranges from 35 to 88 cm and occurs at a shallower depth for soils formed in bar deposits. Soil PDI (profile development index) values range from 61.4 to 80.8 for the Qt3 soils (Table 2).

By comparison, soils formed on the Qt3 terrace surface near Ainsa reflect soil formation under a much wetter subhumid climate. Soil development primarily consists of very thick soil Bt horizons with patchy to nearly continuous coatings of clay along pores, ped faces and gravels. B horizon thickness on the Qt3 surface exceeds 300 cm.



There is no carbonate accumulation in Qt3 terrace soils along the upper reach of the Rio Cinca valley due to the high effective soil moisture. The only soil described on the Qt3 surface near Ainsa has a PDI value of 105.1 (Table 2). The higher value reflects the greater degree of soil development that has occurred under the more humid climate at Ainsa sector relative to soils forming near the Albalate sector.

Soil age estimates for the Qt3 were based on the soil chronofunction developed by Lewis et al. (2009) and the PDI values calculated for the five soils described near Albalate. We did not include the Ainsa Qt3 soil because its more humid soil environment is not compatible with the soil chronofunction developed for soils in more arid settings. Soil age estimates (based on each PDI value; Table 2) ranged from 291 to 565 ka; mean age was  $401 \pm 117$  ka (Table 1). The Qt3 soils were better developed than soils formed on the Qt5 surface, which is approximately 178 ka (Table 2).

#### **4.4 Incision rates**

River incision rates have been calculated by comparing the vertical separation (m) and the elapsed time (ka) between successive terrace strath surfaces. For this level of analysis, we considered that strath formation and the deposition of the corresponding alluvium are generally synchronous in time. The terrace sequences at Ainsa (kilometer 50 from headwaters; upper valley reach) and at Albalate (kilometer 125 from headwaters; lower valley reach) sectors (Fig. 6) were selected because of the extensive presence of well-preserved terrace remnants in both areas (Figs. 3B, C, 4D, F).

Differential mean heights, elapsed mean time and mean incision rates for the selected

sets of coupled terraces are summarized in Table 5. Uncertainties in numerical dating were also considered to present maximum and minimum fluvial incision rates (Table 5).

Considering mean incisions from the coupled successions Qt3-Qt7, Qt7-Qt9 and Qt9-active channel, we proposed that a regional mean fluvial incision rate of  $0.47 \text{ m ka}^{-1}$  occurred during the Middle and Late Pleistocene. The spatial and temporal patterns of river incision also show some singularities. Rates of fluvial incision decreased downstream from Ainsa to Albalate; mean incision rates were  $0.56 \text{ m ka}^{-1}$  at Ainsa and  $0.38 \text{ m ka}^{-1}$  at Albalate. Additionally, the mean incision rate obtained from the coupled succession Qt3-Qt7 was  $0.38 \text{ m ka}^{-1}$  at Ainsa and  $0.20 \text{ m ka}^{-1}$  at Albalate (Table 5). For the coupled succession Qt7-Qt9, values were  $0.76 \text{ m ka}^{-1}$  and  $0.61 \text{ m ka}^{-1}$ , respectively. The coupled Qt9-active channel succession indicates incision of  $0.54 \text{ m ka}^{-1}$  at Ainsa and  $0.33 \text{ m ka}^{-1}$  at Albalate. These results clearly indicate that incision rates were higher on the upper reach relative to the lower reach over the considered time intervals.

The temporal pattern of variation in incision rates along the Cinca River valley reflects important changes during the Middle and Late Pleistocene. These changes are well observed in the Albalate sector, where the more complete sequence of terraces is preserved (Table 5). The Middle Pleistocene coupled Qt3-Qt5 terraces reflects an incision rate of  $0.11 \text{ m ka}^{-1}$ . By comparison, the incision rate of  $0.24 \text{ m ka}^{-1}$  was considerably higher during the Middle-Late Pleistocene transition for the coupled Qt5-Qt6 terraces. The Cinca River attained the highest incision rates during the Late Pleistocene. Pairing the Qt6-Qt7 terraces gives an incision rate of  $0.74 \text{ m ka}^{-1}$  and the

coupled Qt7-Qt8 terraces yields the maximum calculated rate of 1.48 m ka<sup>-1</sup>. For the coupled Qt8-Qt9 terraces and the Qt9-Active channel, incision rates were substantially lower: 0.26 m ka<sup>-1</sup> and 0.33 m ka<sup>-1</sup>, respectively (Table 5; Fig. 8). Time-related trends in incision rates along the Ainsa sector, where the number of couples of terraces is less, were similar (Table 5; Fig. 8). As a consequence, the temporal incision pattern shows very low rates over the Middle Pleistocene, a gradual increase until the beginning of the Late Pleistocene (maximum rates at 60-50 ka) and then a gradual decrease to the present.

Additionally, taking into account the proposed paleomagnetic dates for Qt1 (Jaramillo event, 999-1070 ka) and Qt2 (reversed period previous Jaramillo event, 780-999 ka) in the Albalate sector (Table 1), we can tentatively estimate mean incision rates of 0.06 m ka<sup>-1</sup> and 0.34 m ka<sup>-1</sup> for the coupled terraces of Qt2-Qt3 and Qt1-Qt2, respectively (Table 5; Fig. 8).

## 5. Discussion

Landscape evolution and regional fluvial incision reflects an integration between uplift and climate (e.g., Whipple and Tucker, 1999; Gibbard and Lewin, 2009; Wegmann and Pazzaglia, 2009; Westaway et al., 2009; Stokes et al., 2012; Pazzaglia, 2013). Some studies have defined the geodynamic state (e.g., Lewis et al., 2000; Cloetingh et al., 2002; Garcia-Castellanos et al., 2003; Gunnell et al., 2008; Casas-Sainz and de Vicente, 2009; Fernández-Lozano et al., 2011) and the climate evolution based on fluvial records (Fuller et al., 1998; Lewis et al., 2009; Benito et al. 2010; García-Ruiz et al., 2013; Whitfield et al., 2013; Sancho et al., 2015) during the Quaternary in NE Spain.

The results presented above provide an opportunity to better understand the factors constraining regional and temporal fluvial incision patterns in the NE Iberian Peninsula.

### **5.1 Regional fluvial incision pattern**

The regional pattern of the Cinca River incision can be basically defined by (i) the well-marked vertical separation between successive terrace straths, (ii) the near-parallel terrace strath profiles, and (iii) the westward migration of the Cinca River through time. The calculated mean river incision rate in the Cinca River valley (Pyrenees and Ebro Basin) during the Middle and Late Pleistocene was  $0.47 \text{ m ka}^{-1}$ . This rate is similar to channel incision rates of  $\leq 1 \text{ m ka}^{-1}$  for mountainous regions where commonly paired and extensive terraces occur (Wegmann and Pazzaglia, 2009). A maximum incision rate of  $0.98 \text{ m ka}^{-1}$  in the Miranda basin (Upper Ebro river valley), also within the Pyrenees, has been indicated by Soria-Jáuregui et al. (2016). Although regional data on river incision rates across the Iberian Peninsula are limited, the topographic pattern of river incision in the Pyrenees and the Ebro Basin is clearly different than those observed in the nearby Iberian Range (Giachetta et al., 2015) or in other extensive Iberian Tertiary basins drained by rivers flowing into the Atlantic Ocean. Mean fluvial incision rates of  $0.065 \text{ m ka}^{-1}$  from the terrace sequence of the Arlanzón River (Duero Basin) have been reported by Moreno et al. (2012), and a figure of  $0.05 \text{ m ka}^{-1}$  for terraces in different river valleys in the Central Tagus Basin has been roughly estimated by Silva et al. (2013, 2016). Fluvial incision rates of  $0.07\text{--}1 \text{ m ka}^{-1}$  (Cunha et al., 2005, 2008) and  $0.13\text{--}0.53 \text{ m ka}^{-1}$  (Martins et al., 2009) have been calculated from terrace sequences in the Lower Tagus River basin.

### 5.1.1 Vertical separation between strath terraces

In the Cinca River valley, vertical separation between couples of adjacent terrace straths ranged from approximately 10 to 50 m near Albalate (Table 5). Uplift must be sufficiently high to produce well marked altitudinal separation between terraces (Wang et al., 2015). He et al. (2015) obtained incision rates of 0.62-1.83 m ka<sup>-1</sup> for terraces developed in rapidly uplifting mountainous areas (SE Tibetan Plateau), clearly higher than in the Cinca River valley under post-tectonic conditions. Many studies have demonstrated how long-term incision rates serve as a proxy for bedrock uplift rates (Merritts et al., 1994; Bridgland, 2000; Pazzaglia and Brandon, 2001; Wegmann and Pazzaglia, 2002; Bridgland and Westaway, 2008).

There are three regional geodynamic mechanisms that likely explain the geomorphic expression of the incision of the Cinca River. First, post-orogenic lithosphere uplift in the northeastern Iberian margin could be at least partially attributed to isostatic adjustment resulting from crustal thickening influenced by pre-existing faults (Casas-Sainz and de Vicente, 2009; Fernández-Lozano et al., 2011).

Second, lithosphere uplift could also be related to erosional unloading in the Pyrenees and the Ebro Basin after the connection of the drainage system with the Mediterranean Sea at the end of the Late Miocene (Coney et al., 1996; Vergés et al., 1998; Waltham et al., 2000; Garcia-Castellanos et al., 2003; Gibson et al., 2007; Stange et al., 2016; Garcia-Castellanos and Larrasoña, 2015). Erosional denudation has prevailed for at least the last 10 Ma in the Central Pyrenees (Coney et al., 1996; Fitzgerald et al., 1999; Garcia-Castellanos et al., 2003; Gibson et al., 2007) and

thermochronologic (U-Th/He) data indicate uniformly low rates (0.2 mm/yr) (Gibson et al., 2007). On the other hand, it should be noted that the thickness of sedimentary fill in the north-central sector of the Ebro basin during the Late Oligocene and Early Miocene exceeded 5,000 m and consequently caused important flexural load effects on the lithosphere (Gaspar-Escribano et al., 2001). Considering the topography of the youngest Tertiary rocks (Pérez-Rivarés et al., 2002) preserved in the Central Ebro Basin (Monte Oscuro and San Caprasio, 812 m a.s.l.) and the altitude of the active Cinca channel close to the confluence into the Ebro River (Mequinenza Reservoir, 80 m a.s.l.), a denudation of 750 m must be considered as a minimum to explain the erosional rebound. The flexural isostatic compensation of the eroded materials from the Ebro basin is considered by Garcia-Castellanos and Larrasoña (2015) to be the major force driving fluvial incision and topographic development.

A third factor that could also modulate Quaternary regional uplift required to develop the terrace sequence of the Cinca River is the occurrence of a warm, buoyant asthenosphere perhaps related to adjacent active crustal extension and volcanism in northeastern Spain (Lewis et al., 2000). This is further supported by Janssen et al. (1993) who presented a model of subsidence in the Valencia Trough and associated uplift in the eastern Iberian margin during the Pliocene. Mantle dynamics during post-orogenic stages may also account for the uplift in the Pyrenees and the Ebro southern foreland basin (Stange et al., 2016). However, Garcia-Castellanos and Larrasoña (2015) considered forces related to mantle flow to have a minor role in building the post-tectonic topography of the Ebro basin.

Finally, although numerical dates to establish correlations are very limited, the broadly uniform altimetry of the staircase terrace sequences in the valleys of the main tributaries flowing into the Ebro River from the Pyrenees (Noguera Ribagorzana, Cinca, Alcanadre and Gállego rivers, from east to west) is noticeable (Gutiérrez and Peña, 1994).

#### 5.1.2 Near-parallel strath profiles

In addition to vertical separation between terrace straths of the Cinca River, near-parallel concave-upward terrace profiles were also clearly demonstrated (Fig. 6). Steady regional crustal uplift would drive uniform fluvial incision and invariant incision rates, resulting in parallel terrace longitudinal profiles (Schlunegger and Hinderer, 2001; Pazzaglia, 2013). As a consequence, we postulate a trend to a uniform uplift rate over the Pleistocene in NE Iberia.

A weak trend upstream divergence of strath profiles was also observed. The upstream divergence among Qt3, Qt7 and Qt9 profiles includes a decrease in terrace gradient from Qt3 to Qt9 terraces (Fig. 6). The stream gradient controls both the stream-power and the transport capacity (Hack, 1973) through flow velocity. On the other hand, bedload movement by rolling is related to flow velocity near the streambed (Chorley et al., 1984). As a consequence, gravel-size transport is directly related to channel gradient. Considering the more representative strath terraces along the Cinca River valley (Qt3, Qt7 and Qt9), the maximum grain size ( $D_{max}$ ) ( $34\pm6$  cm,  $34\pm9$  cm and  $29\pm12$  cm, respectively) remained near-uniform (Fig. 5). Then, flow velocity during deposition of the Qt3, Qt7 and Qt9 alluvium remained nearly uniform. Clast-size

averages of the entire set of terraces overlapped within uncertainties. A decrease in the maximum grain size ( $D_{max}$ ) along each terrace profile has also been observed (Fig. 5), which indicates that the hydraulic shear stress decreases proportionally to the gradient of the stream (Schumm, 1977; Larue, 2008; Pazzaglia, 2013).

The upstream divergence of terrace straths along the Cinca River indicates differential regional uplift as a primary driver of terrace formation rather than changes in fluvial erosivity and incision driven by cycles of climate transition (Whipple et al., 1999; Whipple and Tucker, 1999). Several mechanisms may be involved to explain the postulated differential regional uplift: (i) a reinforced uplift in response to a higher denudation rate affecting the Pyrenees as a function of topographic relief (Champagnac et al., 2008; Stange et al., 2016); (ii) an isostatic rebound of the Central Pyrenees related to lithospheric thickening (Zeyen and Fernández, 1994; Gunnel et al., 2008), supported by an important negative Bouguer anomaly associated with the Pyrenean building (Casas et al., 1997); and (iii) a flexural rebound related to removal of Pleistocene glaciers in the headwaters of the Cinca-Cinqueta valley (Belmonte, 2014).

### *5.1.3 Migration westward of the Cinca River*

The Cinca River has markedly migrated to the west during incision, based on the distribution of mapped terrace surfaces (Fig. 3B, C; Appendix 1). The maximum lateral westward displacement reached 7 km between Qt3 and Qt7 in the Albalate section of the lower Cinca River valley. Westward migration ceased from the Qt7 terrace ( $61 \pm 4$  ka). The observed arrangement of the terraces extends to the regional scale because it is common in the Pyrenean side of the central Ebro Basin, as has been shown in the



Noguera Ribagorzana River valley (Peña-Monné, 1983; Sancho, 1988), to the east of the Cinca River, in the Alcanadre River valley (Rodríguez, 1986; Calle et al., 2013), and the Gállego River valley (Benito, 1989), to the west of the Cinca River.

Lateral migration can play an important role in the river incision rates because it maintains an unconstrained width of the valley over time and, as a consequence, the obtained river incision rates could be comparable. Fluvial incision into bedrock is basically proportional to the stream power and inversely proportional to the channel width (Howard et al., 1994; Sklar and Dietrich, 1998; Brocard and van der Beek, 2006). Terrace treads of the Qt1 to Qt7 terraces consist of wide aggradational surfaces (Figs. 3B, C, 4; Appendix 1). For example, the Qt3 valley section is approximately a minimum of 5.5 km wide at Barbastro and the Qt7 valley width reaches a minimum of 4.5 km at Santa Lecina. Subsequent to formation of the Qt7 terrace, the river valley becomes narrower and the available width to accommodate subsequent terraces decreases (Qt8 and Qt9) to a maximum of 2 km between Monzón and Fraga. Considering the uniform lithology of the geological bedrock (Schanz and Montgomery, 2016), the higher erosivity from Qt7 to Qt9 (the pair Qt7-Qt8 yields a rate of  $1.48 \text{ m ka}^{-1}$ ), therefore, could be, at least partially, related to restrictions imposed by valley width.

Channel migration and the related asymmetry of Pleistocene terraces may also be controlled by the regional westward tilt of Oligocene-Miocene bedrock in the Ebro basin. Strata dip gently westward ( $5^\circ$  maximum) along the western margin of the Cinca River valley (Sancho, 1988). This regional tilting requires an uplift mechanism more active in eastern Iberia, with tilting related to the uplift of the rift shoulder (including the eastern Pyrenees, the Catalan Coastal Ranges and the adjacent Ebro Basin)

(Janssen et al., 1993; Casas-Sainz and de Vicente, 2009) accompanying the opening of the western Mediterranean margin during the Neogene (Roca and Desegaulx, 1992; Coney et al., 1996; Lewis et al., 2000). The uniform altimetry of the sequences of terraces in the main Pyrenean tributaries of the Ebro River, from east to west, however, suggests a cessation of differential uplift in the Mediterranean shoulder from at least the Mid Pleistocene. As a consequence, increased eastern uplift plays an indirect role in the westward migration of the Cinca River through the tilting bedrock.

## ***5.2 Changes in incision rates over the last 1 Ma***

Analysis of incision rates indicates that non-uniform river incision in the Cinca River valley has occurred over the last 1 Ma (Table 5; Fig. 8). Temporal changes in fluvial incision rates are particularly well established in the lower reach of the valley where the terrace sequence is preserved. Changes in river incision rates over time can be linked to changes in uplift rates (He et al., 2015; Ruszkiczay-Rüdiger et al., 2016) and/or climate driven changes in erosivity (e.g., Whipple et al., 1999; Schlunegger and Hinderer, 2001; Hartshorn et al., 2002; Zaprowski et al., 2005; Yang et al., 2011).

Using currently available data, there is no evidence of variability in the tectonic uplift rate of NE Iberia during the Mid-Late Pleistocene (Casas-Sainz and de Vicente, 2009; Fernández-Lozano et al., 2011); however, strong variability in climate has been well established, particularly during the Penultimate and the Last Glacial cycles at regional scale (Lewis et al., 2009; Sancho et al., 2015). Lewis et al. (2009) linked fluvial aggradation phases during the Mid-Late Pleistocene in the Cinca River valley with enhanced periods of glacier outwash that produced high discharges of water and

2007  
2008  
2009  
2010  
2011  
2012  
2013  
2014  
2015  
2016  
2017  
2018  
2019  
2020  
2021  
2022  
2023  
2024  
2025  
2026  
2027  
2028  
2029  
2030  
2031  
2032  
2033  
2034  
2035  
2036  
2037  
2038  
2039  
2040  
2041  
2042  
2043  
2044  
2045  
2046  
2047  
2048  
2049  
2050  
2051  
2052  
2053  
2054  
2055  
2056  
2057  
2058  
2059  
2060  
2061  
2062  
2063  
2064  
2065

745  
746  
747  
748  
749  
750  
751  
752  
753  
754

sediment yield down-stream along the valley. Therefore, a close correlation was established between alluvial deposition and cold stages: Qt5 correlates to MIS6, Qt6 to the MIS5b-5c transition, Qt7 to MIS4, Qt8 to the H5 event and Qt9 to the Younger Dryas period (Lewis et al., 2009). Periods of higher fluvial incision would be likely during interstadial stages with a lower sediment supply and greater water discharge activated by retreating glaciers. There is a broad agreement that correlates valley aggradation to cold climates and river incision to transitional and warm climates (e.g., Chorley et al., 1984; Fuller et al., 1998; Vandenberghe and Maddy, 2001; Macklin et al., 2002; Pan et al., 2003; Vandenberghe, 2003; Gao et al., 2008; Wegmann and Pazzaglia, 2009).

755  
756  
757  
758  
759  
760  
761  
762  
763  
764  
765  
766

Regional incision also reflects cycles of variable glacial meltwater discharge over time as a function of the extension and retreat of the Cinca and Cinqueta valley glaciers. For example, the last maximum glacier advance in the Central Pyrenees was at 60-70 ka (MIS4) (Sancho et al., 2003; Lewis et al., 2009) and correlates well with the Qt7 terrace (Lewis et al., 2009), the most important geomorphological marker along the valley. The Cinca-Cinqueta glacier system reached a length of 25 km at this time. Subsequent glacier retreat would produce increased runoff that, in turn, would accelerate fluvial downcutting resulting in higher rates of river incision (Dethier, 2001). As result, the highest expected fluvial incision rates would occur during the timing of the couple Qt7-Qt8 (from 61±4 ka to 47±4 ka) following the last maximum glacier extension. In fact, this is the case; the incision rate was 1.48 m ka<sup>-1</sup> in the lower reach of the Cinca River valley (Albalate sector). Nonetheless, the decrease in valley width after Qt7 formation

must also be considered to explain this high incision rate, as has been previously indicated.

The incision rates obtained between Qt6 ( $97\pm 16$  ka) and Qt7 ( $61\pm 4$  ka) formation ( $0.74$  m  $\text{ka}^{-1}$ ) and between Qt9 and the active channel (last  $11\pm 1$  ka) ( $0.33$  m  $\text{ka}^{-1}$ ) are also remarkable. Significantly lower incision rates were deduced during the Mid-Pleistocene (e.g.,  $0.11$  m  $\text{ka}^{-1}$  between Qt3 and Qt5 in the Albalate sector), resulting from less intense glacial pulses and/or higher valley width maintained as a consequence of the migration westward of the Cinca River. Our results do not well match the acceleration in river incision during the Mid-Pleistocene Revolution at the global scale (Bridgland and Westaway, 2008). Regardless, the general temporal pattern in the lower reach of the Cinca River valley (Albalate sector) can be extrapolated to the upper reach (Ainsa sector).

Finally, agreement between denudation and isostatic rebound must also be considered (Garcia-Castellanos and Lasarrosa, 2015). The increase in fluvial entrenchment would involve a lowering of the regional drainage and an increased denudation between Qt6 ( $97\pm 16$  ka) and Qt8 ( $47\pm 4$  ka), which in turn implies a higher erosional isostatic uplift during this period demonstrating a positive feedback loop (Finnegan et al., 2008; Westaway et al., 2009; Schlunegger et al., 2011).

## 6. Conclusions

Incision rates derived from the regional distribution of a well-preserved sequence of staircase terraces along 170 km in the Cinca River valley have been developed for the last 1 Ma in the Central Pyrenees and the adjacent Ebro basin (NE Iberia). The

sequence is composed of ten well separated terraces (from Qt1 to Qt10) formed under post-orogenic geodynamics and glacial/ interglacial climate conditions. Formation of this extensive paired cyclic terrace sequence was climatically controlled and required a significant regional uplift. Combined results from terrace mapping, height of terrace straths and profiles, and numerical ages of the alluvium overlying terrace straths allow analysis of the spatial and temporal river incision patterns and provides several interpretation of mechanisms involved:

1) Considering coupled successions of the more extensive terraces (Qt3-Qt7, Qt7-Qt9 and Qt9-active channel), the mean fluvial incision rate along the Cinca River during the Middle and Late Pleistocene was approximately around  $0.47 \text{ m ka}^{-1}$ . This incision rate was slightly greater in the upper reach of the valley (Ainsa sector) ( $0.56 \text{ m ka}^{-1}$ ) than in the lower reach (Albalate sector) ( $0.38 \text{ m ka}^{-1}$ ). In addition, the highest incision rate ( $1.48 \text{ m ka}^{-1}$ ) in the lower reach of the valley occurred during Qt7-Qt8 terrace formation (61-47 ka) and the lowest rate ( $0.11 \text{ m ka}^{-1}$ ) occurred during Qt3-Qt5 terrace formation (401-178 ka).

2) The spatial distribution of incision rates showed a near-uniform pattern of fluvial down-cutting along the Cinca River valley. Nearly parallel terrace profiles were driven by a near-uniform regional uplift activated by (i) tectonic uplift related to lithospheric thickening and (ii) isostatic rebound in response to regional denudation unloading, after the connection of the Ebro Basin with the Mediterranean Sea. Subtle upstream divergence of strath profiles appears to be governed by a differential increased uplift in the upper mountainous reach of the valley (Axial Pyrenees) rather than by a decrease in climate-driven erosivity with time.

3) Temporal incision rates show a non-uniform time pattern throughout the last 1 Ma.

The highest incision rate ( $1.48 \text{ m ka}^{-1}$ ) occurred during Qt7-Qt8 terrace formation (61-47 ka). This highest rate appears to be related to a combination of (i) the high glacial meltwater discharge after the last maximum advance of the Pyrenean Cinca-Cinqueta glacier system and (ii) by the deactivation of migration westward of the Cinca River, favouring a lower width of the valley. Currently, the Cinca River is not in equilibrium and modern incision continues.

Incision rates calculated in the Ebro Basin draining to the Mediterranean Sea are much higher than rates for the Iberian rivers flowing into the Atlantic Ocean. Undoubtedly, the post-tectonic geodynamic setting of NE Iberia, the denudation triggered after the exorheism of the Ebro basin and the Pleistocene glacier evolution in the Pyrenees play a determinant role in explaining this difference in landscape evolution at the Iberian scale.

Additional regional studies of staircase terrace sequences are necessary to validate the proposed spatial and temporal patterns and to confirm the combined effect of uplift and climate on fluvial incision rates and the landscape evolution of NE Iberia.

## 7. Acknowledgments

This paper is a tribute to Dr. Claudia J. Lewis, who died prematurely when we were developing the manuscript. At the picture, Claudia guiding a field-trip to the Cinca River Valley included in the program of the V Spanish Geological Congress (2004). The paper collects much of the hard work performed cooperatively between 1998 and 2012. Research was funded by grants from the National Geographic Society, the

National Science Foundation (EAR-0088714), U.S. Army Research Office grants DAAD19-03-1-0159 and W911NF-09-1-0256, the Spanish Ministry of Education, and a Fulbright Senior Scholar grant to C. Lewis. We thank the Institute of Geophysics and Planetary Physics and Laboratory Directed Research and Development (LDRD) at Los Alamos National Laboratory for additional funding. The Desert Research Institute provided GPS equipment. Laboratory soil analyses were carried out at the Desert Research Institute. We thank John Geissman, Bet Beamud and Miguel Garcés for use of the paleomagnetic labs at the University of New Mexico (Albuquerque) and the Institute of Earth Sciences “Jaume Almera” CSIC-UB (Barcelona, Spain). We thank Marta Lopez for combining all of our data into a Geographic Information System. This study is a contribution of the PALEOQ Research Group (Aragon Government and European Social Fund) and IUCA (University of Zaragoza). Authors thank two anonymous reviewers for their comments that helped improve the manuscript. Thanks are also due to the Editor Prof. Andy Plater for the final refinement of the manuscript.

## References

- Antón, L., Rodés, A., De Vicente, G., Pallàs, R, Garcia-Castellanos, D., Stuart, F.M., Braucher, R. and Bourlès, D. (2012). Quantification of fluvial incision in the Duero Basin (NW Iberia) from longitudinal profile analysis and terrestrial cosmogenic nuclide concentrations. *Geomorphology*, 165-166, 50-61.
- Bailey, R.C. and Halls, H.C. (1984). Estimate of confidence in paleomagnetic directions derived from mixed remagnetization circle and direct observational data. *Journal of Geophysics*, 54, 174-182.

2302  
2303  
2304 856 Barnolas, A., Gil-Peña, I. and Martín-Alfageme, S. (2009). Mapa Geológico de Pirineos a  
2305  
2306 escala 1:400.000. IGME-BRGM.  
2307 857  
2308  
2309  
2310 858 Belmonte, A. (2014). Geomorfología del Macizo de Cotiella (Pirineo oscense):  
2311  
2312 859 Cartografía, evolución paleoambiental y dinámica actual. PhD thesis, University of  
2313  
2314 860 Zaragoza, 580 p.  
2315  
2316  
2317  
2318 861 Beltrán, A. (1985). Historia de Aragón, vol. II. Guara Editorial, 183 p. Zaragoza.  
2319  
2320  
2321 862 Benito, G. (1989). Geomorfología de la Cuenca Baja del río Gállego. PhD thesis,  
2322  
2323 863 University of Zaragoza, 764 p.  
2324  
2325  
2326  
2327 864 Benito, G., Sancho, C., Peña, J.L., Machado, M.J. and Rhodes, E.J. (2010). Large-scale  
2328  
2329 865 karst subsidence and accelerated fluvial aggradation during MIS6 in NE Spain: climatic  
2330  
2331 866 and paleohydrological implications. Quaternary Science Reviews, 29, 2694-2704.  
2332  
2333  
2334  
2335 867 Birkeland, P.W. (1999). Soils and Geomorphology. Oxford University Press, New York.  
2336  
2337 868 430 p.  
2338  
2339  
2340 869 Bridgland, D.R. (2000). River terrace systems in north-west Europe: an archive of  
2341  
2342 870 environmental change, uplift and early human occupation. Quaternary Science  
2343  
2344 Reviews, 19, 1293-1303.  
2345 871  
2346  
2347  
2348 872 Bridgland, D. and Westaway, R. (2008). Climatically controlled river terrace staircases:  
2349  
2350 873 A worldwide Quaternary phenomenon. Geomorphology , 98, 285-315.  
2351  
2352  
2353  
2354 874 Brocard, G.Y. and van der Beek, P.A. (2006). Influence of incision rate, rock strength,  
2355  
2356 875 and bedload supply on bedrock river gradients and valley-flat widths: field-based  
2357  
2358  
2359  
2360



2361  
2362  
2363  
2364 876 evidence and calibrations from western Alpine rivers (southeast France). In Willet, S.D.,  
2365  
2366 877 Hovious, N., Brandon, M.T. and Fisher, D.M. (Eds.). Tectonics, Climate and Landscape  
2367  
2368 878 Evolution. Geological Society of America, Special Paper 398, 101-126.  
2369  
2370  
2371 879 Bull, W.B. (1991). Geomorphic Response to Climatic Change. Oxford University Press,  
2372  
2373 880 326 p. New York.  
2374  
2375  
2376  
2377 881 Burbank, D.W. and Anderson, R.S. (2001). Tectonic Geomorphology. Blackwell, 274  
2378  
2379 882 Malden.  
2380  
2381  
2382 883 Calle, M., Sancho, C., Peña, J.L., Cunha, P., Oliva-Urcia, B. and Pueyo, E. (2013). La  
2383  
2384 884 secuencia de terrazas cuaternarias del río Alcanadre (provincia de Huesca):  
2385  
2386  
2387 885 caracterización y consideraciones paleoambientales. Cuadernos de Investigación  
2388  
2389 886 Geográfica, 39, 159-178.  
2390  
2391  
2392 887 Casas, A., Kearey, P., Rivero, L. and Adam, C.R. (1997). Gravity anomaly map of the  
2393  
2394 888 Pyrenean region and a comparison of the deep geological structure of the western and  
2395  
2396  
2397 889 eastern Pyrenees. Earth and Planetary Science Letters, 150, 65-78.  
2398  
2399  
2400 890 Casas-Sainz, A.M. and de Vicente, G. (2009). On the tectonic origin of Iberian  
2401  
2402 891 topography. Tectonophysics, 474, 214-235.  
2403  
2404  
2405  
2406 892 Champagnac, J.D., van der Beek, P., Diraison, G. and Dauphin, S. (2008). Flexural  
2407  
2408 893 isostatic response of the Alps to increased Quaternary erosion recorded by foreland  
2409  
2410 894 basin remnants, SE France. Terra Nova, 20, 213-220.  
2411  
2412  
2413  
2414 895 Chorley, R.J., Schumm, S.A. and Sugden, D.E. (1984). Geomorphology. Methuen, 605 p.  
2415  
2416 896 London.  
2417  
2418  
2419

- Cloetingh, S. and Willett, S.D. (2013). TOPO-EUROPE: Understanding of the coupling between the deep Earth and continental topography. *Tectonophysics*, 602, 1-14.
- Cloetingh, S., Burov, E., Beekman, F., Andeweg, B., Andriessen, P.A.M., Garcia-Castellanos, D., de Vicente, G. and Vegas, R. (2002). Lithospheric folding in Iberia. *Tectonics*, 21, 5-1-5-26.
- Coney, P.J., Muñoz, J.A., McClay, K.R. and Evenchick, C.A. (1996). Syntectonic burial and post-tectonic exhumation of the southern Pyrenees foreland fold-and-thrust belt. *Journal of the Geological Society, London*, 153, 9-16.
- Costa, E., Garcés, M., López-Blanco, M., Beamud, E., Gómez-Paccard, M. and Larrasoaña, J.C. (2010). Closing and continentalization of the South Pyrenean foreland basin (NE Spain): magnetochronological constraints. *Basin Research*, 26, 904-917.
- Cunha, P.P., Martins, A.A., Daveau, S., Friend, P. (2005). Tectonic control of the Tejo river fluvial incision during the late Cenozoic, in Ródão-central Portugal (Atlantic Iberian border). *Geomorphology*, 64, 271-298.
- Cunha, P.P., Martins, A.A., Huot, S., Murray, A.S. and Raposo, L. (2008). Dating the Tejo river lower terraces in the Ródão area (Portugal) to assess the role of tectonics and uplift. *Geomorphology*, 102, 43-54.
- Cunha, P.P., Almeida, N., Aubry, T., Martins, A.A., Murray, S.A., Buylaert, J.P., Sohbati, R., Raposo, L. and Rocha, L. (2012). Records of human occupation from Pleistocene river terrace and aeolian sediments in the Arneiro depression (Lower Tejo River, central eastern Portugal). *Geomorphology*, 165-166, 78-90.

2479  
2480  
2481  
2482 918 Dethier, D.P. (2001). Pleistocene incision rates in the western United States calibrated  
2483 using lava Creek B tephra. *Geology*, 29, 783-786.  
2484 919  
2485  
2486  
2487 920 Dubar, M. and Semah, F. (1986). Paleomagnetic data bearing on the age of high terrace  
2488 deposits (Durance Sequence) in Alpine valleys of southeastern France. *Quaternary*  
2489 921  
2490 Research, 25, 387-391.  
2491 922  
2492  
2493  
2494  
2495 923 Duval, M., Sancho, C., Calle, M., Guilarte, V. and Peña-Monné, J.L. (2015). On the  
2496 potential of the ESR dating method applied to optically bleached quartz grains in  
2497 924  
2498 sedimentary fluvial environments: some examples from the Early Pleistocene terraces  
2499 925  
2500 of the Alcanadre river (Ebro basin, Spain). *Quaternary Geochronology*, 29, 58-69.  
2501 926  
2502  
2503  
2504  
2505 927 Fernández-Lozano, J., Sokoutis, D., Willingshofer, E., Muñoz-Martín, A., De Vicente, G.  
2506 and Cloetingh, S., (2011). Análisis integrado de la topografía y anomalías gravimétricas  
2507 928  
2508 en la Península Ibérica: nuevas metodologías en modelación análoga. *Revista de la*  
2509 929  
2510 Sociedad Geológica de España, 24, 153-171.  
2511 930  
2512  
2513  
2514  
2515 931 Finnegan, N.J., Hallet, B., Montgomery, D.R., Zeitler, P.K., Stone, J.O., Anders, A.M. and  
2516 Yuping, L. (2008). Coupling of rock uplift and river incision in the Namche Barwa-Gyala  
2517 932  
2518 Peri massif, Tibet. *Geological Society of America Bulletin*, 120, 142-155.  
2519 933  
2520  
2521  
2522  
2523 934 Fisher, R. (1953). Dispersion on a sphere. *Proceedings of the Royal Society of London*.  
2524 Series A. Mathematical and Physical Sciences, 217, 295-305.  
2525 935  
2526  
2527  
2528 936 Fitzgerald, P.G., Muñoz, J.A., Coney, P.J. and Baldwin, S.L. (1999). Asymmetric  
2529 exhumation across the Pyrenean orogen: implications for the tectonic evolution of a  
2530 collisional orogen. *Earth and Planetary Science Letters*, 173, 157-170.  
2531 937  
2532  
2533 938  
2534  
2535  
2536  
2537

2538  
2539  
2540 939 Fuller, I.C., Macklin, M.G., Lewin, J., Passmore, D.G. and Wintle, A.G. (1998). River  
2541  
2542 response to high-frequency climate oscillations in southern Europe over the past 200  
2543 940  
2544 k.y. *Geology*, 26, 275-278.  
2545 941  
2546  
2547  
2548 942 Gao, H., Liu, X., Pan, B., Wang, Y., Yu, Y. and Li, J. (2008). Stream response to  
2549  
2550 Quaternary tectonic and climatic change: Evidence from the upper Weihe River,  
2551 943  
2552 central China. *Quaternary International*, 186, 123-131.  
2553 944  
2554  
2555  
2556 945 Garcia-Castellanos, D., Vergés, J., Gaspar-Escribano, J. and Cloetingh, S. (2003).  
2557  
2558 946 Interplay between tectonics, climate, and fluvial transport during the Cenozoic  
2559  
2560 evolution of the Ebro Basin (NE Iberia). *Journal of Geophysical Research*, 108, 2347,  
2561 947  
2562 doi:10.1029/2002JB002073.  
2563 948  
2564  
2565  
2566 949 Garcia-Castellanos, D. and Larrasoana, J.C. (2015). Quantifying the post-tectonic  
2567  
2568 950 topographic evolution of closed basins: The Ebro basin (northeast Iberia). *Geology*,  
2569  
2570 43, 663-666.  
2571 951  
2572  
2573  
2574 952 García-Ruiz, J.M., Martí-Bono, C., Peña-Monné, J.L., Sancho, C., Rhodes, E.J., Valero-  
2575  
2576 953 Garcés, B., González-Sampériz, P. and Moreno, A. (2013). Glacial and fluvial deposits in  
2577  
2578 954 the Aragón Valley, central-western Pyrenees: chronology of the Pyrenean late  
2579  
2580 Pleistocene glaciers. *Geografiska Annaler: Series A, Physical Geography*, 95, 15-32.  
2581 955  
2582  
2583  
2584 956 Gaspar-Escribano, J. M., van Wees, J. D., ter Voorde, M., Cloetingh, S., Roca, E.,  
2585  
2586 957 Cabrera, L., Muñoz, J. A., Ziegler, P. A. and Garcia-Castellanos, D. (2001). Three-  
2587  
2588 958 dimensional flexural modelling of the Ebro Basin (NE Iberia). *Geophysical Journal*  
2589  
2590 *International*, 145, 349-367.  
2591 959  
2592  
2593  
2594  
2595  
2596

2597  
2598  
2599  
2600  
2601  
2602  
2603  
2604  
2605  
2606  
2607  
2608  
2609  
2610  
2611  
2612  
2613  
2614  
2615  
2616  
2617  
2618  
2619  
2620  
2621  
2622  
2623  
2624  
2625  
2626  
2627  
2628  
2629  
2630  
2631  
2632  
2633  
2634  
2635  
2636  
2637  
2638  
2639  
2640  
2641  
2642  
2643  
2644  
2645  
2646  
2647  
2648  
2649  
2650  
2651  
2652  
2653  
2654  
2655

Giachetta, E., Molin, P., Scotti, V.N. and Faccena, C. (2015). Plio-Quaternary uplift of the Iberian Chanin (central-eastern Spain) from landscape evolution experiments and river profile modeling. *Geomorphology*, 246, 48-67.

Gibbard, P. and Cohen, K.M. (2008). Global chronostratigraphical correlation table for the last 2.7 million years. *Episodes*, 31, 243-247.

Gibbard, P.L. and Lewin, J. (2009). River incision and terrace formation in the late Cenozoic of Europe. *Tectonophysics* 474, 41-55.

Gibson, M., Sinclair, H.D., Lynn, G.J. and Stuart, F.M. (2007). Late- to post-orogenic exhumation of the Central Pyrenees revealed through combined thermochronological data and modeling. *Basin Research*, 19, 323-334.

Gil Garbi, H, 2017. Los depósitos cuaternarios en el sector central de la Cuenca del Ebro: Arquitectura sedimentaria, paleokarst, su interacción con la sedimentación y cronología. PhD thesis, University of Zaragoza, 354 p.

Gil, H., Luzón, A., Soriano, M.A., Casado, I., Pérez, A., Yuste, A., Pueyo, E.L. and Pocoví, A. (2013). Stratigraphic architecture of alluvial-aeolian systems developed on active karst terrains: an Early Pleistocene example from the Ebro Basin (NE Spain). *Sedimentary Geology*, 296, 122-141.

Gile, L.H., Hawley, J.H. and Grossman, R.B. (1981). Soils and geomorphology in the basin and range area of Southern New Mexico-guidebook to the desert project. New Mexico Bureau of Mines and Mineral Resources, Socorro, NM. Memoir 39, 222 p.

2656  
2657  
2658  
2659 980 Gunnell, Y., Zeyen, H. and Calvet, M. (2008). Geophysical evidence of a missing  
2660  
2661 981 lithospheric root beneath the Eastern Pyrenees: Consequences for post-orogenic uplift  
2662  
2663 982 and associated geomorphic signatures. *Earth and Planetary Science Letters*, 276, 302-  
2664  
2665 983 313.  
2666  
2667  
2668  
2669 984 Gutiérrez, M. and Peña, J.L. (1994). Depresión del Ebro. In Gutiérrez, M. (Ed.).  
2670  
2671 985 *Geomorfología de España*, 305-349. Ed. Rueda. Madrid.  
2672  
2673  
2674 986 Hack, J.T. (1973). Stream-profile analysis and stream-gradient index. *Journal Research*  
2675  
2676 987 *U.S. Geological Survey*, 1, 421-429.  
2677  
2678  
2679  
2680 988 Harden, J.W. (1982). A quantitative index of soil development from field descriptions:  
2681  
2682 989 examples from a soil chronosequence in central California. *Geoderma*, 28, 1-28.  
2683  
2684  
2685 990 Harden, J.W. and Taylor, E.M. (1983). A quantitative comparison of soil development in  
2686  
2687 991 four climatic regimes. *Quaternary Research*, 20, 342-359.  
2688  
2689  
2690  
2691 992 Hartshorn, K., Hovius, N., Dade, W.B. and Slingerland, R.L. (2002). Climate-driven  
2692  
2693 993 bedrock incision in an active mountain belt. *Science*, 297, 2036-2038.  
2694  
2695  
2696 994 He, Z., Zhang, X., Bao, S., Qiao, Y., Sheng, Y., Liu, X., He, X., Yang, X., Zhao, J., Liu, R. and  
2697  
2698  
2699 995 Lu, C. (2015). Multiple climatic cycles imprinted on regional uplift-controlled fluvial  
2700  
2701 996 terraces in the lower Yalong River and Anning River, SE Tibetan Plateau.  
2702  
2703 997 *Geomorphology*, 250, 95-112.  
2704  
2705  
2706 998 Howard, A.D., Dietrich, W.E. and Seidl, M.A. (1994). Modeling fluvial erosion on  
2707  
2708  
2709 999 regional to continental scales. *Journal of Geophysical Research* 99 (B7), 13,971-13,986.  
2710  
2711  
2712  
2713  
2714

2715  
2716  
2717  
1000 Jacobson, R.B., Elston, D. P. and Heaton, J.W. (1988). Stratigraphy and magnetic  
2718  
2719  
1001 polarity of the high terrace remnants in the upper Ohio and Monongahela rivers in  
2720  
2721  
1002 West Virginia, Pennsylvania, and Ohio. Quaternary Research, 29, 216-232.  
2722  
2723  
2724  
2725  
1003 Janssen, M.E., Torné, M., Cloetingh, S. and Banda, E. (1993). Pliocene uplift of the  
2726  
2727  
1004 eastern Iberian margin: inferences from quantitative modelling of the Valencia Trough.  
2728  
2729  
1005 Earth and Planetary Science Letters, 119, 585-597.  
2730  
2731  
2732  
2733  
1006 Kirschvink, J.L. (1980). The least-squares line and plane and the analysis of  
2734  
2735  
1007 palaeomagnetic data. Geophysical Journal of the Royal Astronomical Society, 62, 699-  
2736  
2737  
1008 718.  
2738  
2739  
2740  
2741  
1009 Larue, J.P. (2008). Tectonic influence on the Quaternary drainage evolution on the  
2742  
2743  
1010 northwestern margin of the French Central Massif: the Cruese valley example.  
2744  
2745  
1011 Geomorphology, 93, 398-420.  
2746  
2747  
2748  
2749  
1012 Lewis, C., McDonald, E., Sancho, C., Peña, J.L. and Rhodes, E. (2009). Climatic  
2750  
2751  
1013 implications of correlated Upper Pleistocene glacial and fluvial deposits on the Cinca  
2752  
2753  
1014 and Gállego Rivers (NE Spain) based on OSL dating and soil stratigraphy. Global and  
2754  
2755  
1015 Planetary Change, 67, 141-152.  
2756  
2757  
2758  
2759  
1016 Lewis, C.J., Vergés, J. and Marzo, M. (2000). High mountains in a zone of extended  
2760  
2761  
1017 crust: Insights into the Neogene-Quaternary topographic development of northeastern  
2762  
2763  
1018 Iberia. Tectonics, 19, 86-102.  
2764  
2765  
2766  
2767  
1019 Li, J.J., Fang, X.M., van der Voo, R., Zhu, J.J., Mac Niocaill, C., Ono, Y., Pan, B.T., Zhong,  
2768  
2769  
1020 W., Wang, J.L., Sasaki, T., Zhang, Y.T, Cao, J.X., Kang, S.C. and Wang, J.M. (1997).  
2770  
2771  
2772  
2773

2774  
2775  
2776  
1021 Magnetostratigraphic dating of river terraces: Rapid and intermittent incision by the  
2777  
2778  
1022 Yellow River of the northeastern margin of the Tibetan Plateau during the Quaternary.  
2779  
2780  
1023 Journal of Geophysical Research, 102, 10121-10132.  
2782  
2783  
2784  
1024 Lucha, P., Gutiérrez, F. and Guerrero, J. (2008). Environmental problems and geological  
2785  
1025 implications derived from evaporite dissolution in the Barbastro salt anticline (NE  
2787  
2788  
1026 Spain). Environmental Geology, 53, 1045-1055.  
2789  
2790  
2791  
2792  
1027 Macklin, M.G., Fuller, I.C., Lewin, J., Maas, G.S., Passmore, D.G., Rose, J., Woodward,  
2793  
2794  
1028 J.C., Black, S., Hamlin, R.H.B. and Rowan, J.S. (2002). Correlation of fluvial sequences in  
2795  
2796  
1029 the Mediterranean basin over the last 200 ka and their relationship to climate change.  
2797  
2798  
1030 Quaternary Science Reviews, 21, 1633-1641.  
2799  
2800  
2801  
2802  
1031 Martínez-Peña, M. and Casas-Sainz, A. (2003). Cretaceous-Tertiary tectonic inversion  
2803  
2804  
1032 of the Cotiella Basin (southern Pyrenees, Spain). International Journal of Earth  
2805  
2806  
1033 Sciences, 92, 99-113.  
2807  
2808  
2809  
2810  
1034 Martínez-Peña, B., Casas-Sainz, A. and Millán-Garrido, H. (1995). Palaeostresses  
2811  
2812  
1035 associated with thrust sheet emplacement and related holding folding in the southern  
2813  
2814  
1036 central Pyrennes, Huesca, Spain. Journal of the Geological Society, London, 152, 353-  
2815  
2816  
1037 364.  
2817  
2818  
2819  
2820  
1038 Martins, A.A., Cunha, P.P., Huot, S., Murray, A.S. and Buylaert, J.P. (2009).  
2821  
2822  
1039 Geomorphological correlation of the tectonically displaced Tejo River terraces  
2823  
2824  
1040 (Gavião-Chamusca area, central Portugal) supported by luminescence dating.  
2825  
2826  
1041 Quaternary International, 199, 75-91.  
2827  
2828  
2829  
2830  
2831  
2832



Martins, A.A., Cunha, P.P., Buylaert, J.P., Huot, S., Murray, A.S., Dinis, P., Stokes, M. (2010). K-feldspar IRSL dating of a Pleistocene river terrace sequence of the Lower Tejo River (Portugal, western Iberia). *Quaternary Geochronology*, 5, 176-180.

McDonald, E.V., Reneau, S.L. and Gardner, J.N. (1996). Soil-forming processes on the Pajarito Plateau: Investigation of a soil chronosequence in Rendija Canyon. In: Goff, F., Kues, B.S., Rogers, M.A., McFadden, L.D. and Gardner, J.N. (Eds.), *New Mexico Geological Society Guidebook, 47th Conference*. Socorro, New Mexico, USA, p. 375-382.

Merritts, J., Vicent, R. and Wohl, E. (1994). Long river profiles, tectonism and eustasy: a guide to interpreting fluvial terraces. *Journal of Geophysical Research* 99 (B7), 14031-14050.

Miall, A.D. (1978). Lithofacies types and vertical profile models in braided river deposits: a summary. In: Miall, A.D. (Ed.). *Fluvial sedimentology*. Canadian Society of Petroleum Geologists, Memoir 5, 597-604.

Moreno, D., Falguères, C., Pérez-González, A., Duval, M., Voinchet, P., Benito-Calvo, A., Ortega, A.I., Bahain, J.J., Sala, R., Carbonell, E., Bermúdez de Castro, J.M. and Arsuaga, J.L. (2012). ESR chronology of alluvial deposits in the Arlanzón valley (Atapuerca, Spain): Contemporaneity with Atapuerca Gran Dolina site. *Quaternary Geochronology*, 10, 418-423.

Muñoz, J.A. (2002). The Pyrenees. In Gibbons, W. and Moreno, M.T. (Eds.). *The Geology of Spain*, 370-385. Geological Society, London.

2892  
2893  
2894  
2895  
2896  
2897  
2898  
2899  
2900  
2901  
2902  
2903  
2904  
2905  
2906  
2907  
2908  
2909  
2910  
2911  
2912  
2913  
2914  
2915  
2916  
2917  
2918  
2919  
2920  
2921  
2922  
2923  
2924  
2925  
2926  
2927  
2928  
2929  
2930  
2931  
2932  
2933  
2934  
2935  
2936  
2937  
2938  
2939  
2940  
2941  
2942  
2943  
2944  
2945  
2946  
2947  
2948  
2949  
2950

Muñoz, A., Arenas, C., González, A., Luzón, A., Pardo, G., Pérez, A. and Villena, J. (2002). Ebro basin (northeastern Spain). In Gibbons, W. and Moreno, M.T. (Eds.). The Geology of Spain, 301-309. Geological Society, London.

Pan, B.T., Burbank, D., Wang, Y.X., Wu, G.J., Li, J.J. and Guan, Q.Y. (2003). A 900 ka record of strath terrace formation during glacial-interglacial transitions in northwest China. *Geology*, 31, 957-960.

Pazzaglia, F.J. (2013). Fluvial Terraces. In Wohl, E. (Ed.). *Treatise of Geomorphology*, Volume 9, 379-412. Elsevier.

Pazzaglia, F.J. and Brandon, M.T. (2001). A fluvial record of rock uplift and shortening across the Cascadia forearc high. *American Journal of Science*, 301, 385-431.

Peña-Monné, J.L. (1983). La Conca de Tremp y Sierras Prepirenaicas comprendidas entre los ríos Segre y Noguera Ribagorzana: estudio geomorfológico. Instituto de Estudios Ilerdenses, 373 p., Lleida.

Peña-Monné, J.L. (1994). Cordillera Pirenaica. In Gutiérrez, M. (Ed.). *Geomorfología de España*, 159-225. Rueda, Madrid.

Pérez-Rivarés, J., Garcés, M., Arenas, C. and Pardo, G. (2002). Magnetocronología de la sucesión Miocena de la Sierra de Alcubierre (sector central de la Cuenca del Ebro). *Revista Sociedad Geológica de España*, 15, 3-4.

Pevzner, M.A. (1970). Paleomagnetic studies of Pliocene-Quaternary deposits of Pridniestrovie. *Palaeogeography, Palaeoclimatology, Palaeoecology*, 8, 215-219.

2951  
2952  
2953  
1083 Pueyo, E.L., Garcés, M., Mauritsch, H.J., Lewis, C., Scholger, R., Sancho, C., Molina, R.,  
2954  
2955  
1084 Schnepf, E., Larrasoña, J.C., Parés, J.M., Pocoví, A., Muñoz, A., Valero, B., Millán, H.,  
2956  
2957  
1085 Laplana, C., Oliva, B. and González, P. (2006). Sampling, transportation and magnetic-  
2958  
2959  
1086 free consolidation of extremely soft sediments for paleomagnetic purposes: a  
2960  
2961  
1087 successful "recipe". In Calvo, M., Garcés, M., Gomes, C., Larrasoña, J.C., Pueyo, E. and  
2962  
2963  
1088 Villalaín, J.J. (Eds). MAGIBER I: Paleomagnetismo en la Península Ibérica, 121-128.  
2964  
2965  
2966  
1089 Universidad de Burgos, ISBN: 84-96394-35-2.  
2967  
2968  
2969  
1090 Puigdefábregas, C. and Souquet, P. (1986). Tecto-sedimentary cycles and depositional  
2970  
2971  
1091 sequences of the Mesozoic and Tertiary from the Pyrenees. In Banda, E. and Wickham,  
2972  
2973  
1092 S.M. (Eds.). The Geological Evolution of the Pyrenees, Tectonophysics, 129, 173-203.  
2974  
2975  
2976  
2977  
1093 Ramón, M.J., Pueyo, E.L., Oliva-Urcia, B. and Larrasoña, J.C. (2017). Virtual Directions  
2978  
2979  
1094 in Paleomagnetism: A Global and Rapid Approach to Evaluate the NRM Components.  
2980  
2981  
1095 Frontiers of Earth Science, 5, 1-14.  
2982  
2983  
2984  
2985  
1096 Roca, E. and Desegaulx, P. (1992). Analysis of the geological evolution and vertical  
2986  
2987  
1097 movements in the València trough area, western Mediterranean. Marine and  
2988  
2989  
1098 Petroleum Geology, 9, 167-185.  
2990  
2991  
2992  
2993  
1099 Rodríguez, J. (1986). Geomorfología de las Sierras Exteriores oscenses y su  
2994  
2995  
1100 piedemonte. Instituto de Estudios Altoaragoneses, Huesca, 172 p.  
2996  
2997  
2998  
2999  
1101 Ruskiczay-Rüdiger, Z., Braucher, R., Novothny, A., Csillag, G., Fodor, L., Molnár, G.,  
3000  
3001  
1102 Madarász, B. and ASTER Team (2016). Tectonic and climatic control on terrace  
3002  
3003  
1103 formation: Coupling in situ produced <sup>10</sup>Be depth profiles and luminescence approach,  
3004  
3005  
1104 Danube River, Hungary, Central Europe. Quaternary Science Reviews, 131, 127-147.  
3006  
3007  
3008  
3009

Sancho, C. (1988). Geomorfología de la cuenca baja del río Cinca. PhD thesis, University of Zaragoza, 743 p.

Sancho, C. (1989). Deformaciones asociadas a la actividad diapírica cuaternaria del Anticlinal de Barbastro (provincia de Huesca). Cuaternario y Geomorfología, 3, 35-43.

Sancho, C., Calle, M., Peña-Monné, J.L., Duval, M., Oliva-Urcia, B., Pueyo, E.L., Benito, G. and Moreno, A. (2016). Dating the earliest Pleistocene alluvial terrace of the Alcanadre River: Insights on the landscape evolution of the Ebro Basin (NE Spain). Quaternary International, 407, 86-95.

Sancho, C., Peña, J.L., Lewis, C., McDonald, E. and Rhodes, E. (2003). Preliminary dating of glacial and fluvial deposits in the Cinca River Valley (NE Spain): chronological evidences for the Glacial Maximum in the Pyrenees?. In Ruiz, M.B., Dorado, M., Valdeolmillos, A., Gil, M.J., Bardají, T., Bustamante, I. and Martínez, I. (Eds.). Quaternary climatic changes and environmental crises in the Mediterranean region, 169-173. Universidad de Alcalá-Ministerio de Ciencia y Tecnología-INQUA.

Sancho, C., Arenas, C., Vázquez-Urbez, M., Pardo, G., Lozano, M.V., Peña-Monné, J.L., Hellstrom, J., Ortiz, J.E., Osácar, M.C., Auqué, L. and Torres, T. (2015). Climatic implications of the Quaternary fluvial tufa record in the NE Iberian Peninsula over the last 500 ka. Quaternary Research, 84, 398-414.

Santisteban, J. I. and Schulte, L. (2007). Fluvial networks of the Iberian Peninsula: a chronological framework. Quaternary Science Reviews, 26, 2738-2757.

Schanz, S.A. and Montgomery, D.R. (2016). Lithologic controls on valley width and strath terrace formation. *Geomorphology*, 258, 58-68.

Scheepers, P.J.J. and Zijdeveld, J.D.A. (1992). Stacking in Paleomagnetism: Application to marine sediments with weak NRM, *Geophysical Research Letters*, 19, 1519-1522.

Schlunegger, F. and Hinderer, M. (2001). Crustal uplift in the Alps: why the drainage pattern matters. *Terra Nova*, 13, 425-432.

Schlunegger, F., Norton, K.P. and Zeilinger, G. (2011). Climatic forcing on channel profiles in the Eastern Cordillera on the Coroico region, Bolivia. *The Journal of Geology*, 119, 97-107.

Schumm, S.A. (1977). *The fluvial system*. John Wiley & Sons, 338 p. New York.

Scotti, V.N., Molin, P., Faccenna, C., Soligo, M. and Casas-Sainz, A. (2014). The influence of surface and tectonic processes on landscape evolution of the Iberian Chain (Spain): quantitative geomorphological analysis and geochronology. *Geomorphology*, 206, 37-57.

Sklar, L. and Dietrich, W.E. (1998). River longitudinal profiles and bedrock incision models: stream power and the influence of sediment supply. In: Tinkler, K.J. and Wohl, E.E. (Eds.). *Rivers Over Rock: Fluvial Processes in Bedrock Channels*. Geophysical Monograph, 107. American Geophysical Union, 237-260. Washington D.C.

Silva, P.G., Roquero, E., López-Recio, M., Huerta, P. and Tapias, F. (2013). Statistical approach to the chronosequence of fluvial terraces in the Tagus and Duero basins

(Central Spain). In: Baena, R., Fernández, J.J. and Guerrero, I. (Eds.). El Cuaternario Ibérico: Investigación en el S. XXI, 29-33. Sevilla.

Silva, P.G., Roquero, E., López-Recio, M., Huerta, P. and Martínez-Graña, A.M. (2016). Chronology of fluvial terrace sequences for large Atlantic rivers in the Iberian Peninsula (Upper Tagus and Duero drainage basins, Central Spain). Quaternary Science Reviews doi.org/10.1016/j.quascirev.2016.05.027.

Singer, B.S. (2014). A Quaternary geomagnetic instability time scale. Quaternary Geochronology, 21, 29-52.

Soria-Jáuregui, A., González-Amuchástegui, M.J., Mauz, B. and Lang, A. (2016). Dynamics of Mediterranean late Quaternary fluvial activity: An example from the River Ebro (north Iberian Peninsula). Geomorphology, 268, 110-122.

Stange, K.M., van Balen, R., Vandenberghe, J., Peña, J.L. and Sancho, C. (2013). External controls on Quaternary fluvial incision and terrace formation at the Segre River, Southern Pyrenees. Tectonophysics, 602, 316-331.

Stange, K.M., van Balen, R.T., Garcia-Castellanos, D., Cloetingh, S. (2016). Numerical modelling of Quaternary terrace staircase formation in the Ebro foreland basin, southern Pyrenees, NE Iberia. Basin Research, 28, 124-146.

Starkel, L. (2003). Climatically controlled terraces in uplifting mountain areas. Quaternary Science Reviews, 22, 2189-2198.

Stokes, M., Cunha, P.P. and Martins, A. (2012). Techniques for analysing Late Cenozoic river terrace sequences. Geomorphology, 165, 1-6.

U.S. Soil Survey Staff (1993). Examination and description of soils. Soil Conservation Service. Soil survey manual. U.S. Department of Agriculture Handbook 18. Washington, D.C., USA, Chapter 3.

Vandenbergh, J. (2003). Climate forcing of fluvial system development: an evolution of ideas. *Quaternary Science Reviews*, 22, 2053-2060.

Vandenbergh, J. and Maddy, D. (2001). The response of river systems to climate change. *Quaternary International*, 79, 1-3.

Vergés, J., Marzo, M., Santaaulària, T., Serra-Kiel, J., Burbank, D. W., Muñoz, J. A. and Giménez-Montsant, J. (1998). Quantified vertical motions and tectonic evolution of the SE Pyrenean foreland basin. In: Mascle, A., Puigdefàbregas, C., Luterbacher, H.P. and Fernández, M. (Eds.). *Cenozoic Foreland Basins of Western Europe*, London, Geological Society Special Publications, 134, p. 107-134.

Viveen, W., Schoorl, J.M., Veldkamp, A. and van Balen, R.T. (2014). Modelling the impact of regional uplift and local tectonics on fluvial terrace preservation. *Geomorphology*, 210, 119-135.

Waltham, D.C., Docherty, C., Taberner, C. (2000). Decoupled flexure in the South Pyrenean foreland. *J. Geophys. Res.*, 105, 16,329-16,340.

Wang, X., Vandenbergh, J., Shuangwen, Y., Van Balen, R. and Lu, H. (2015). Climate-dependent fluvial architecture and processes on a suborbital timescale in areas of rapid tectonic uplift: An example from the NE Tibetan Plateau. *Global and Planetary Change*, 133, 318-329.

Wegmann, K.W. and Pazzaglia, F.J. (2009). Late Quaternary fluvial terraces of the Romagna and Marche Apennines, Italy: Climatic, lithologic, and tectonic controls on terrace genesis in an active orogen. *Quaternary Science Reviews*, 28, 137-165.

Westaway, R., Bridgland, D.R., Sinha, R. and Demir, T. (2009). Fluvial sequences as evidence for landscape and climatic evolution in the Late Cenozoic: a synthesis of data from IGCP 518. *Global and Planetary Change*, 68, 237-253.

Whipple, K. and Tucker, G. (1999). Dynamics of the stream-power river incision model: Implications for height limits of mountain ranges, landscape response timescales, and research needs. *Journal of Geophysical Research*, 104, 17661-17674.

Whipple, K.X., Kirby, E. and Brocklehurst, S.H. (1999). Geomorphic limits to climate-induced increases in topographic relief. *Nature*, 401, 39-43.

Whitfield, R.G., Macklin, M.G., Brewer, P.A., Lang, A., Mau, B. and Whitfield (née Maher), E. (2013). The nature, timing and controls of the Quaternary development of the Rio Bergantes, Ebro basin, northeast Spain. *Geomorphology*, 196, 106-121.

Willet, S.D., Hovius, N., Brandon, M.T. and Fischer, D.M. (2006). Introduction. In Willet, S.D., Hovius, N., Brandon, M.T. and Fischer, D.M. (eds.). *Tectonic, climate and landscape evolution*. The Geological Society of America, 398, vii-xi.

Yang, G., Zhang, X., Tina, M., Brierley, G., Chen, A., Ping, Y., Ge, Z., Ni, Z. and Yang, Z. (2011). Alluvial terrace systems in Zhangjiajie of northwest Hunan, China: Implications for climate change, tectonic uplift and geomorphic evolution. *Quaternary International*, 233, 27-39.



Zaprowski, B.J., Pazzaglia, F.J. and Evenson, E.B. (2005). Climatic influences on profile concavity and river incision. *Journal of Geophysical Research*, 110, F03004, doi:10.1029/2004JF000138.

Zeyen, H. and Fernández, M. (1994). Integrated lithospheric modeling combining thermal, gravity, and local isostasy analysis: application to the NE Spanish Geotranssect. *Journal of Geophysical Research*, 99, 18089-18102.

### Figure captions

Figure 1. Location of the Cinca River drainage basin and the Ebro Basin in NE Iberia.

Figure 2. Geological setting of the Cinca River Valley in NE Iberia (A) and geological mapping of the bedrock (adapted from Barnolas et al., 2009) (B).

Figure 3. Distribution of terraces along the Cinca River valley (A). Detailed geomorphological maps and cross-sections of terraces in the Ainsa (B) and Albalate (C) sectors.

Figure 4. Field photographs of terraces in the Cinca River valley: alluvial cover of the terrace Qt7 overlaying Eocene marls near Ainsa (A) and Miocene clays and sandstones near Almudáfar (B); deposits of terrace Qt7 made of massive and cross-stratified gravels near Albalate (C); preserved staircase terrace sequences in the Ainsa (D), Monzón (E) and Binaced (F) sectors.

Figure 5. Grain size trends for Cinca River terrace deposits (Qt3, Qt7, Qt9) decreasing downstream.

Figure 6. Longitudinal profiles of the Cinca River terraces and the active channel.

General parallel profiles with a subtle trend to divergence upstream are observed.

Figure 7. Paleomagnetic analysis. Natural remanent magnetisation of the Cinca

Terraces (A), orthogonal demagnetisation diagrams of selected samples (B) and paleomagnetic means values in the studied terraces (C).

Figure 8. Fluvial incision rates in the Cinca River valley from successive preserved strath

terraces at the upper reach (Ainsa sector) and at the lower reach (Albalate sector) of

the valley. Spatial and temporal differences are clearly identified. Paleomagnetic

timescale and marine isotope stages (adapted from Gibbard and Cohen, 2008) are

included.

### Table captions

Table 1. Terraces, numerical dates and heights at the Albalate and Ainsa sectors of the Cinca River valley.

Table 2. Summary of relative degrees of soil development on the Cinca River terrace surfaces and estimated ages.

Table 3. OSL dates from terraces in the the Cinca River valley (adapted from Lewis et al., 2009).

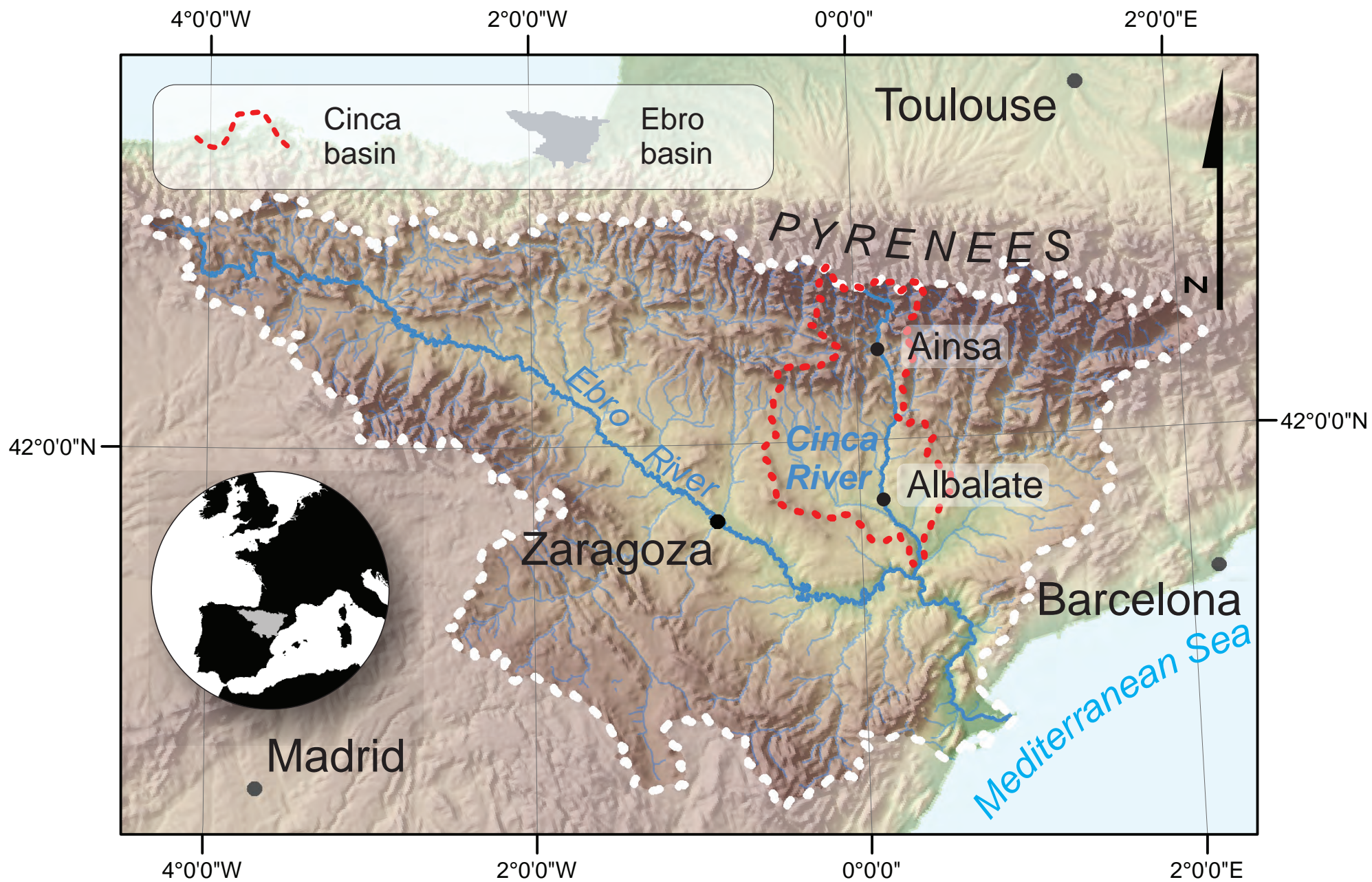
Table 4. Paleomagnetic data. Location and UTM coordinates (T30). n/N; considered/analysed samples. Pol: Polarity. Dec/inc: magnetic declination and inclination and the Fisher (1954) statistical parameters ( $a_{95}$  and K).

Table 5. Fluvial incision rates calculated from coupled preserved terraces in the Cinca River valley. Comparison of incision rates at the Ainsa and Albalate sectors is established. Temporal variations of incision rates at the Albalate sector are also evidenced.

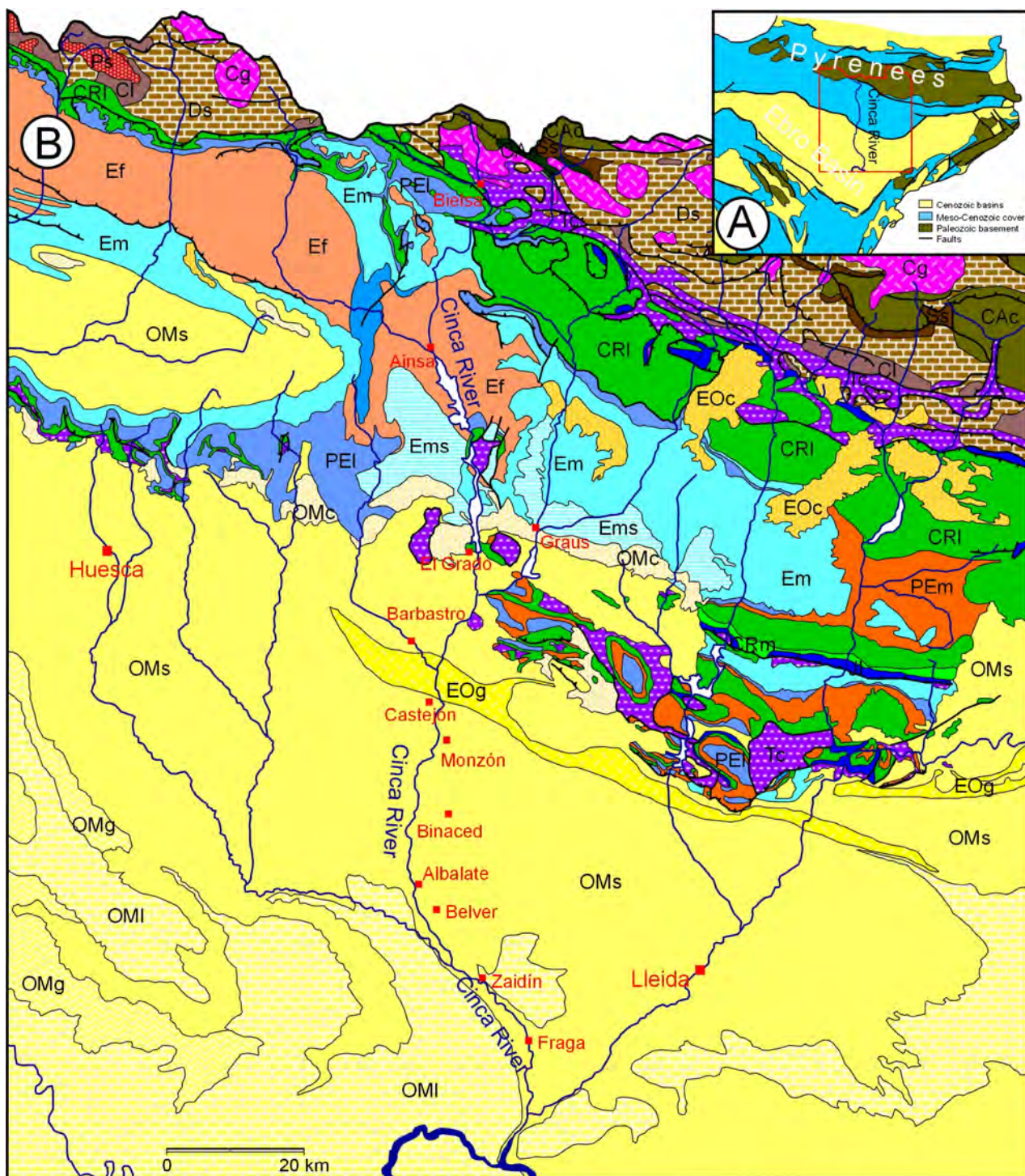
## Appendix captions

Appendix 1. Detailed geological map (including strath terraces) of the Cinca River valley. GPS measurements of elevation of terrace straths and active channel points are also indicated.

Appendix 2. Cinca River terrace strath data measurements and observations. UTM coordinates (latitude and longitude), elevation, substrate lithology (abbreviations: gyp, gypsum; ls, limestone; sst, sandstone), alluvium thickness (m), maximum grain size (Dmax), location and distance from headwaters are indicated. UTM coordinates and strath heights were obtained from a differentially corrected GPS accurate to 1 cm. Measurements from the headwaters of the river were obtained from topographic maps 1:25,000 in scale.







### Tertiary

OMI	Limestones Oligocene-Miocene
OMg	Gypsums Oligocene-Miocene
OMS	Sandstones and claystones Oligocene-Miocene
OMc	Conglomerates Oligocene-Miocene
EOc	Conglomerates Eocene-Oligocene
EOg	Gypsums and salts Eocene-Oligocene
Ef	Flysch Eocene
Em	Marls Eocene

Ems	Marls, sandstones and conglomerates Eocene
PEI	Limestones Paleocene-Eocene
PEm	Marls, claystones and sandstones Paleocene-Eocene

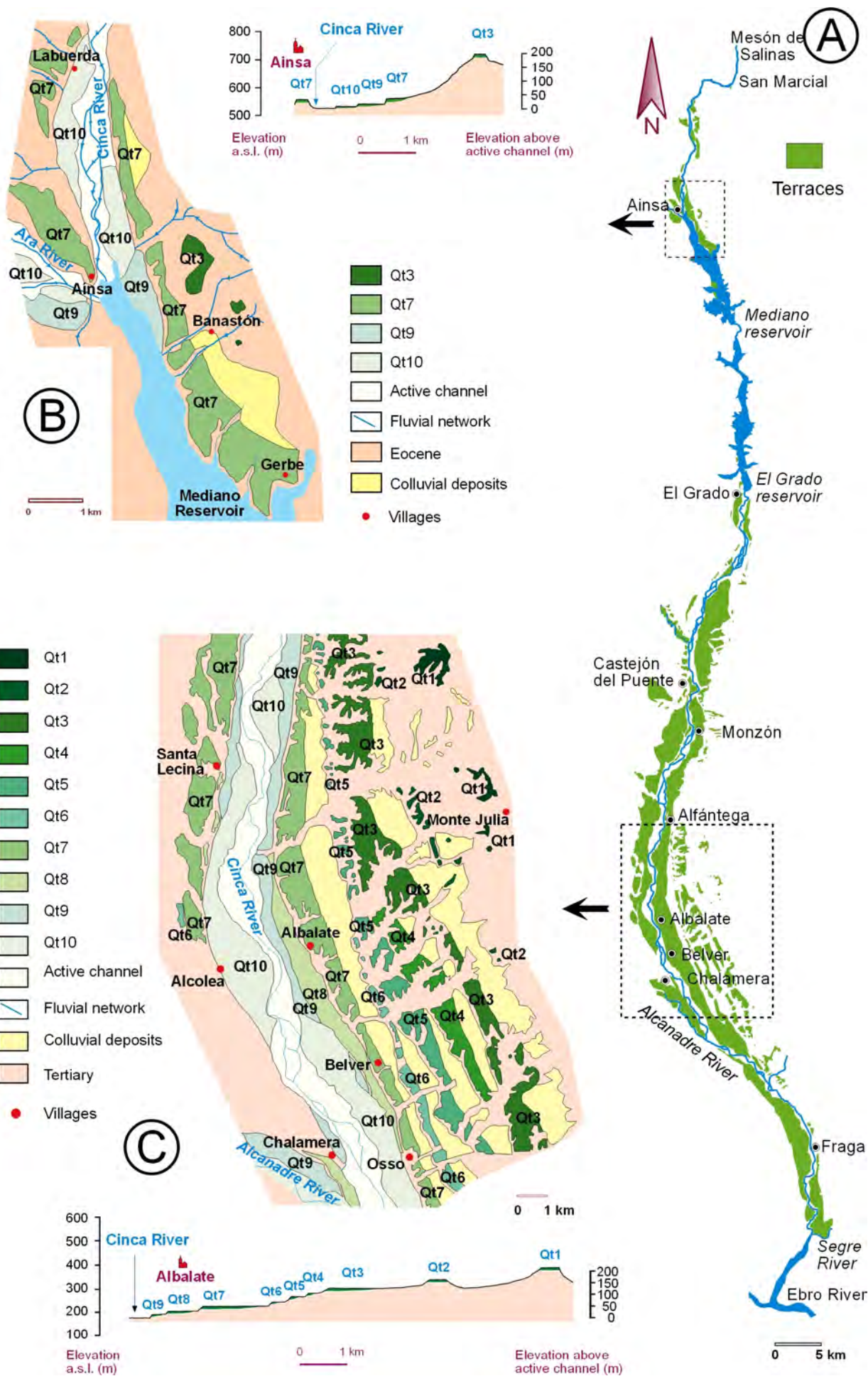
### Mesozoic

CRI	Limestones Upper Cretaceous
CRm	Marls and sandstones Lower Cretaceous
JI	Limestones Jurassic
Tc	Sandstones and claystones Triassic

### Paleozoic

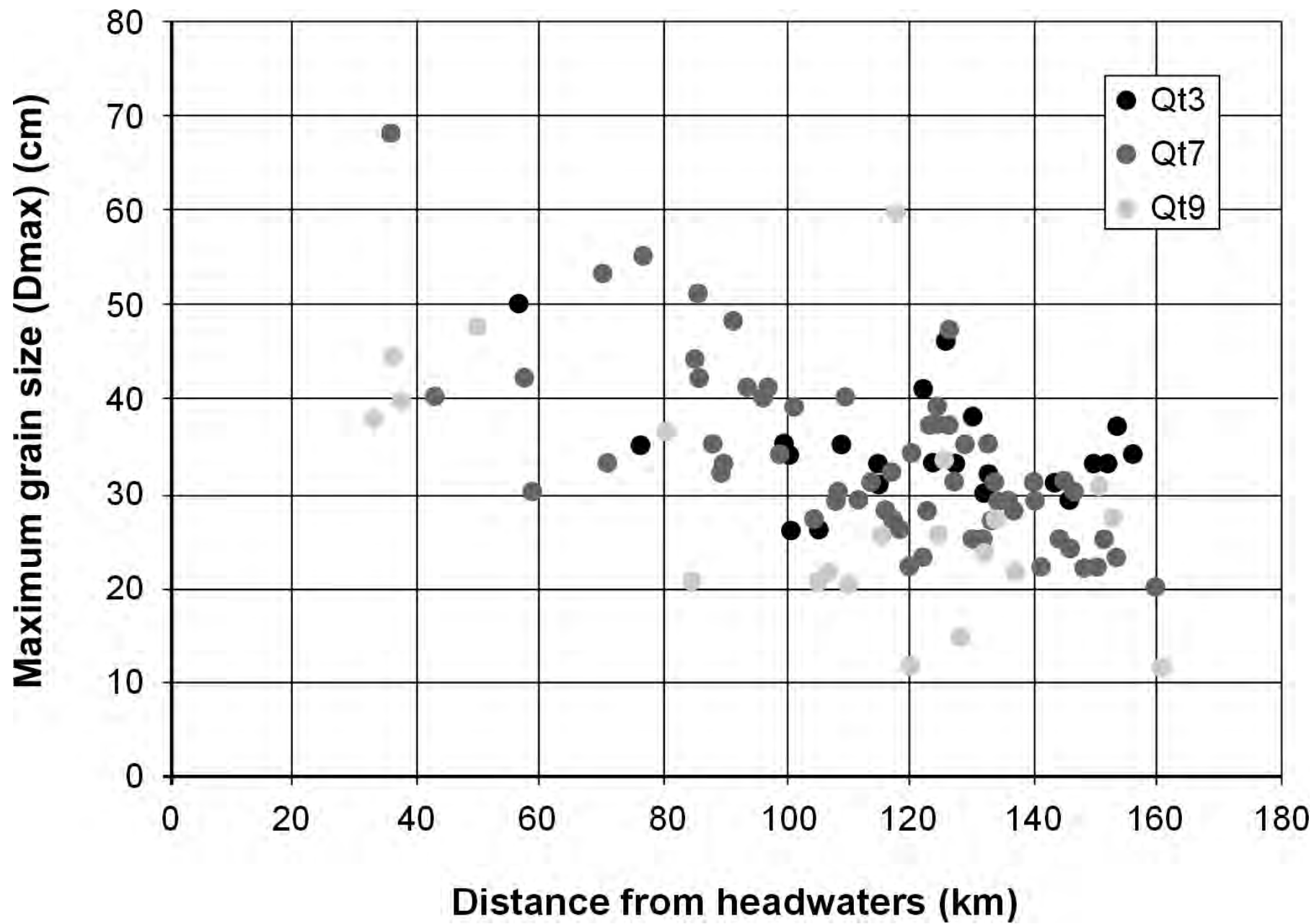
Pa	Andesites Permian
Ps	Sandstones and conglomerates Permian
Cg	Granites Carboniferous
CI	Limestones Carboniferous
Ds	Sandstones and limestones Devonian
Bs	Shales Silurian
CAC	Schists and sandstones Ordovician
CAC	Claystones and sandstones Cambrian



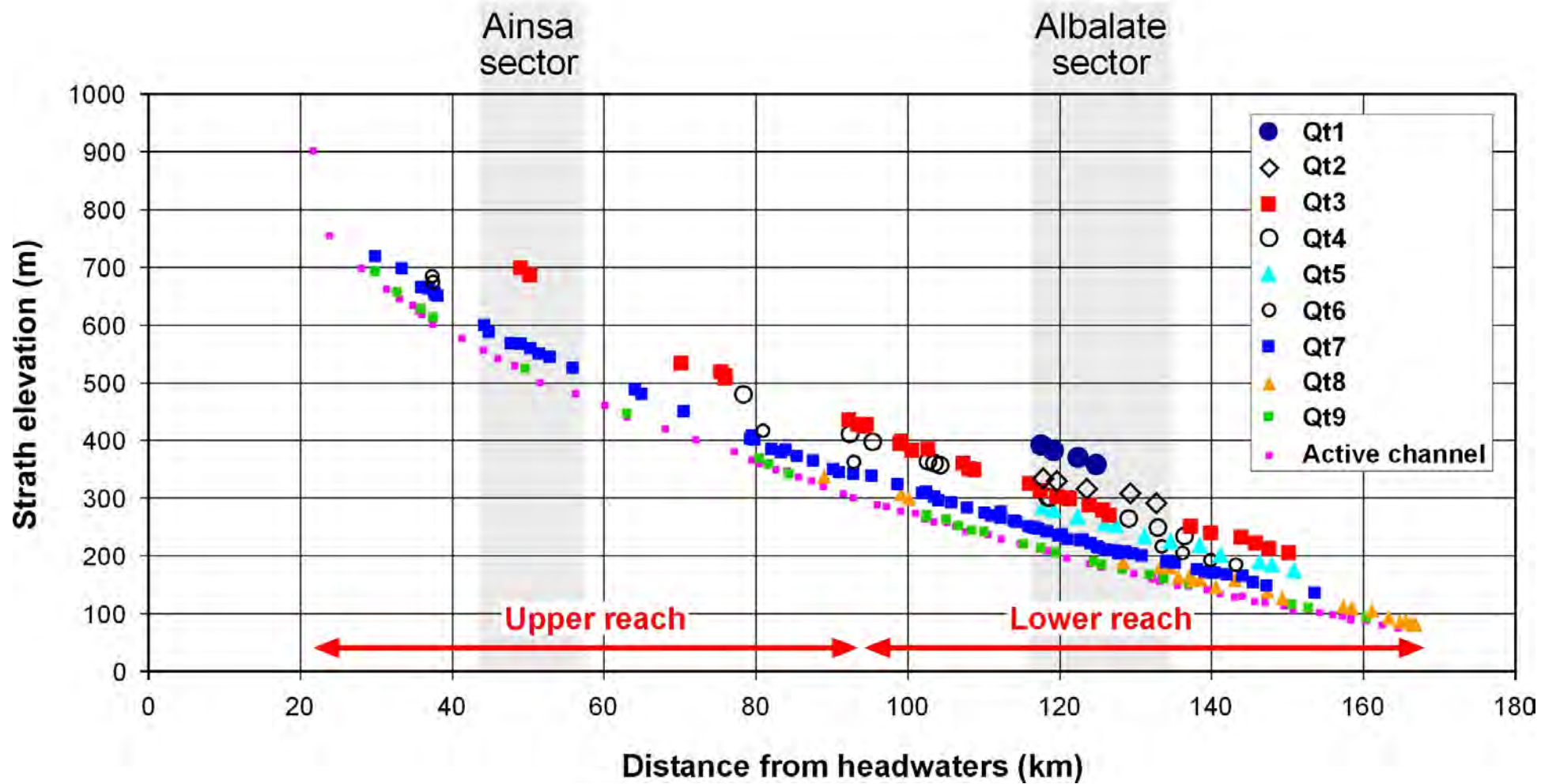


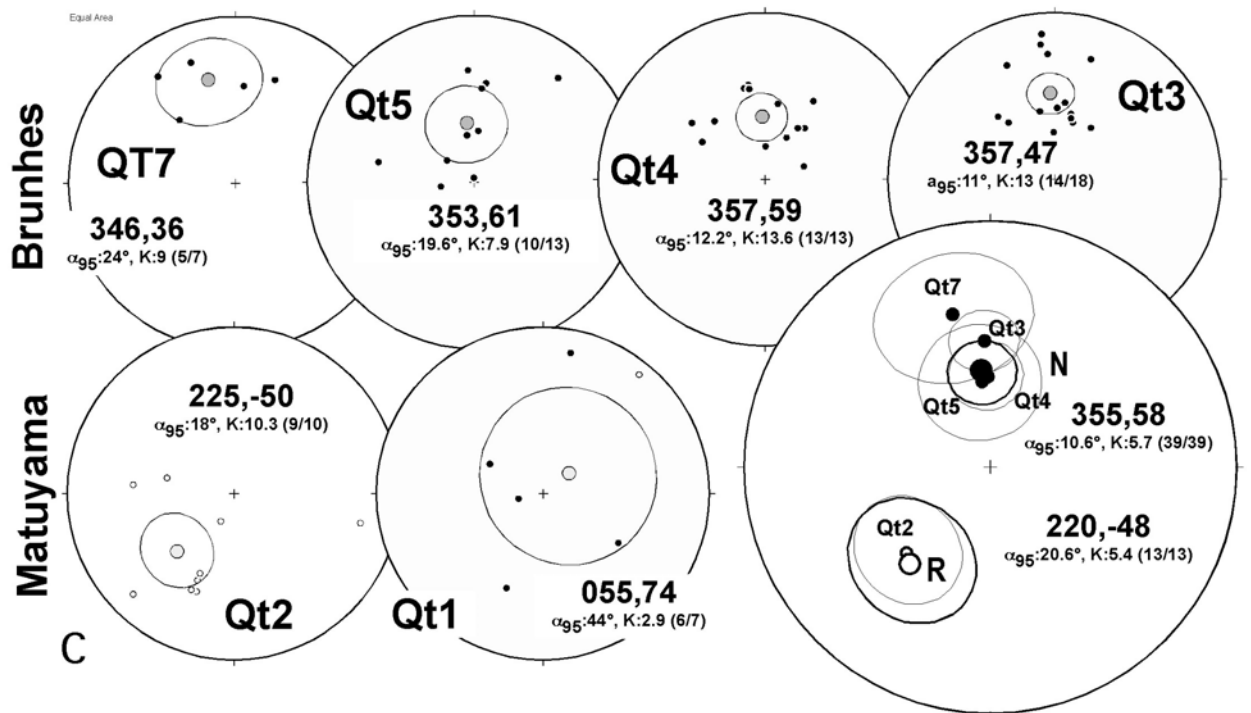
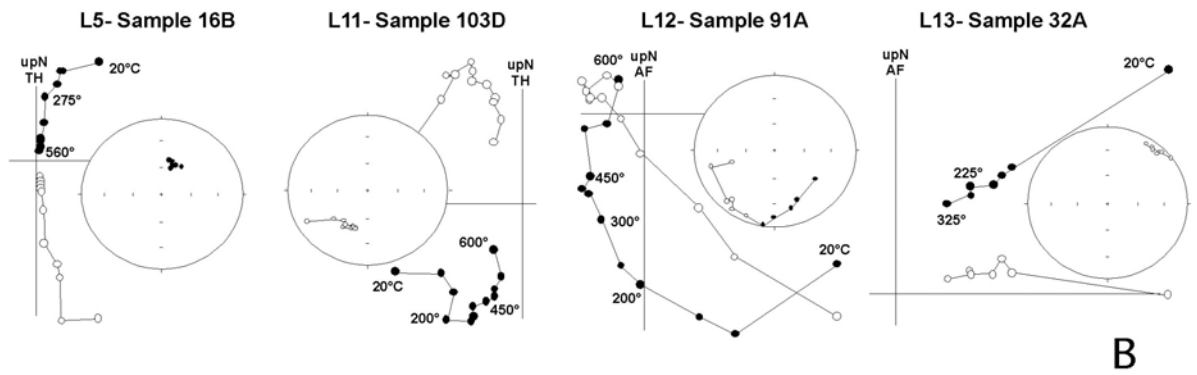
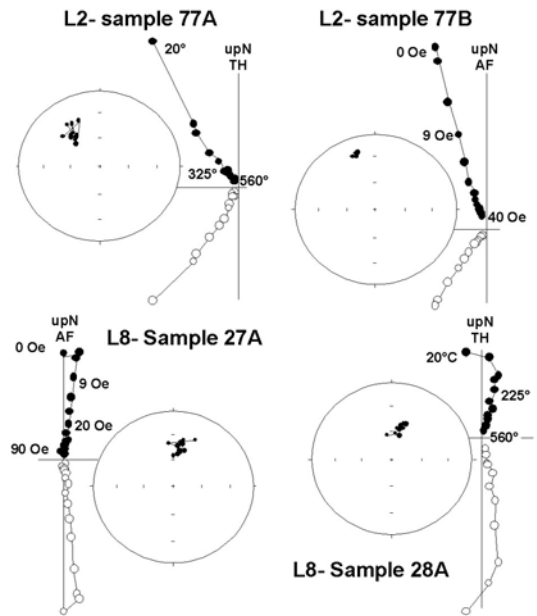
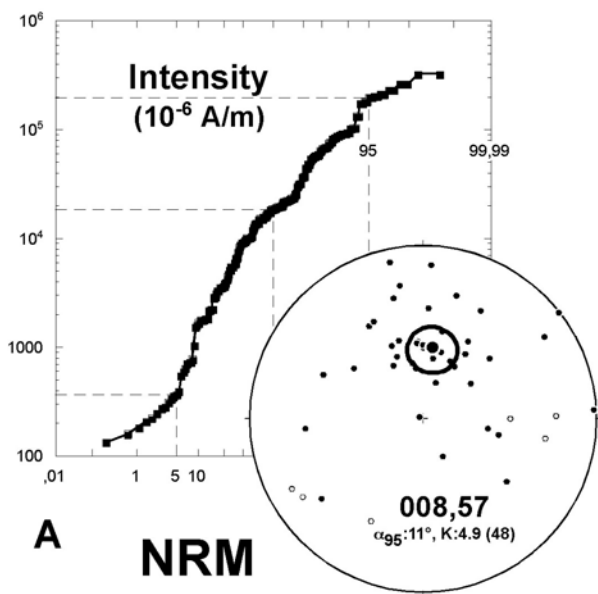


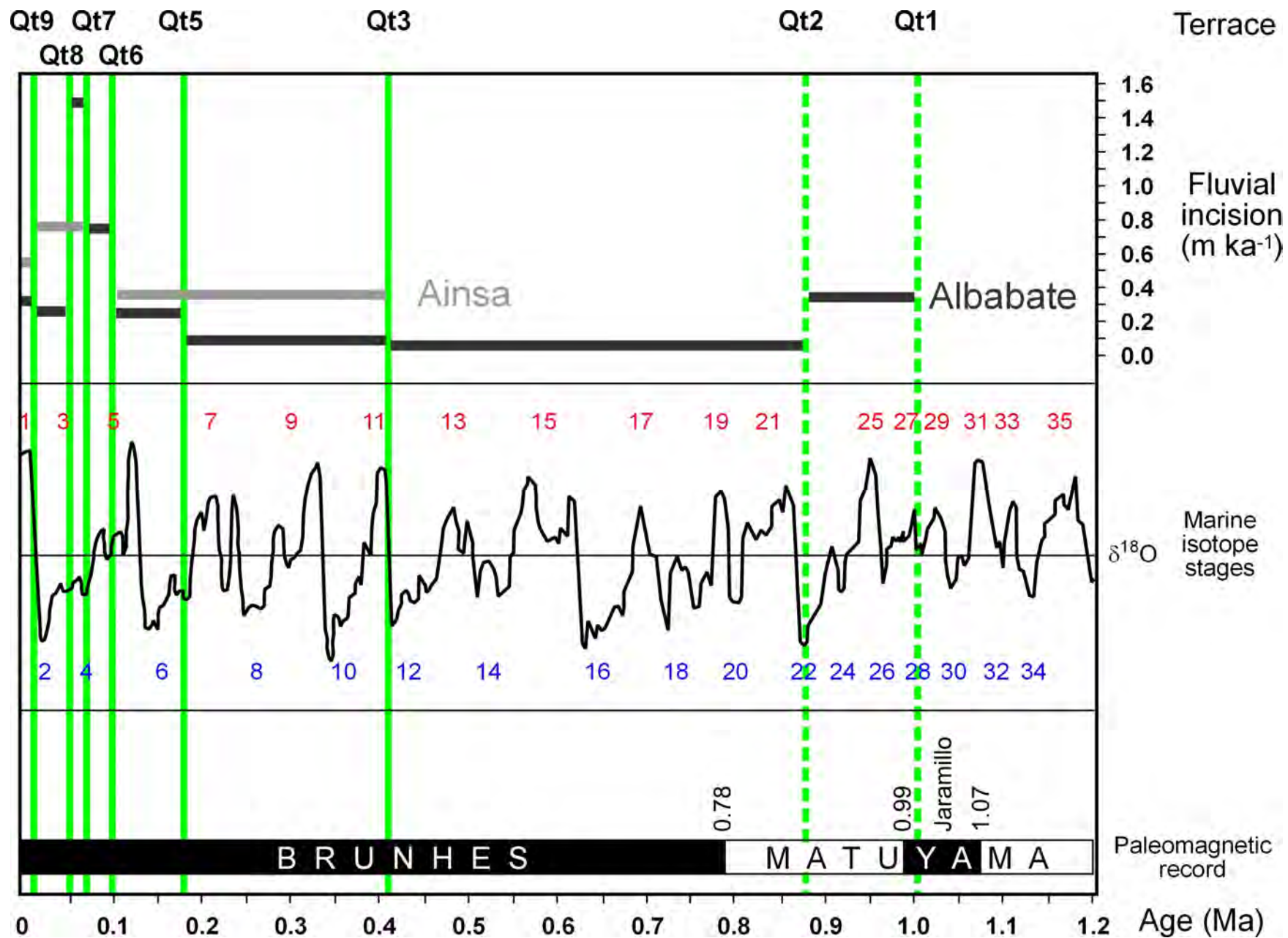






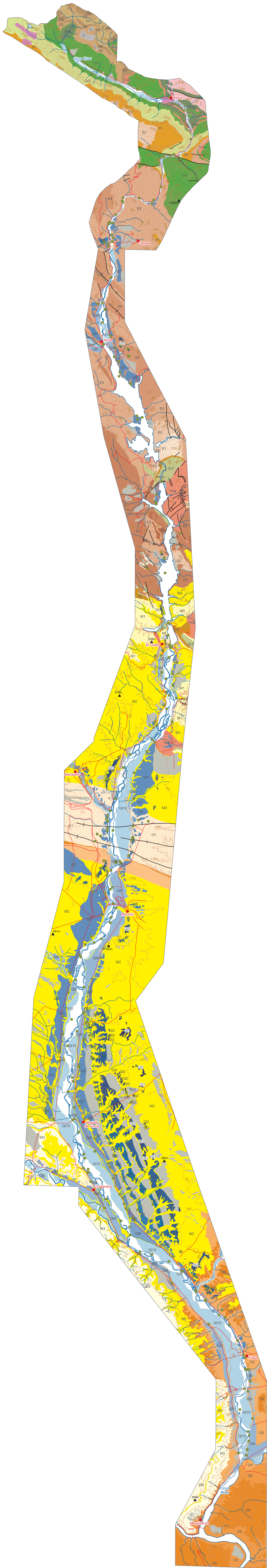






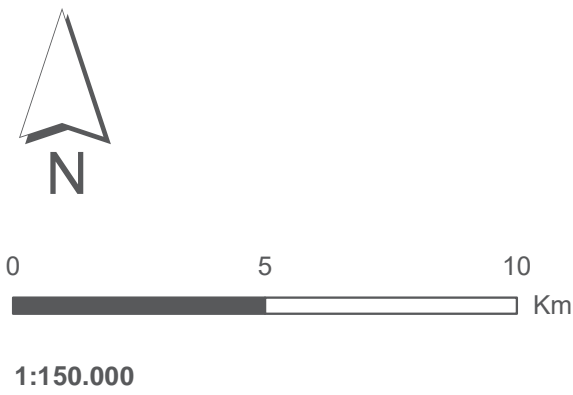


# QUATERNARY FLUVIAL TERRACES IN THE CINCA RIVER VALLEY



## LEGEND

<b>Tertiary</b>		<b>Quaternary</b>	
<b>Miocene</b>		<b>Fluvial terraces</b>	
M1	Conglomerates	Qt1	Qt1
M2	Sandstones and shales	Qt2	Qt2
M3	Limestones and marls	Qt3	Qt3
<b>Oligocene</b>		Qt4	Qt4
O1	Gypsums and shales	Qt5	Qt5
O2	Conglomerates	Qt6	Qt6
O3	Sandstones, shales and conglomerates	Qt7	Qt7
O4	Shales and sandstones	Qt8	Qt8
O5	Sandstones, shales and conglomerates	Qt9	Qt9
O6	Marls and limestones	Qt10	Qt10
<b>Eocene</b>		<b>Others</b>	
E1	Limestones with alveolinids		Active channel
E2	Limestones and marls		Colluviums
E3	Blue marls		Moraines
E4	Turbidites	<b>Other information</b>	
E5	Sandstones, shales and conglomerates		Anticlines
E6	Reef limestones		Synclines
<b>Paleocene</b>			Faults
P1	Limestones and dolostones		Fluvial network
P2	Shales, sandstones and limestones ("Garum")		Roads
<b>Mesozoic</b>			Towns
<b>Cretaceous</b>			Strath elevations (GPS)
Cr1	Limestones		
Cr2	Sandstones		
Cr3	Limestones and dolostones		
<b>Triassic</b>			
Tmk	Shales, gypsums and dolostones		
PTb	Sandstones and conglomerates		
o	Diabases		
<b>Paleozoic</b>			
<b>Carboniferous</b>			
C	Slates and limestones		
<b>Devonian</b>			
D1	Quartzites		
D2	Slates		
D3	Limestones		
γ	Granites		





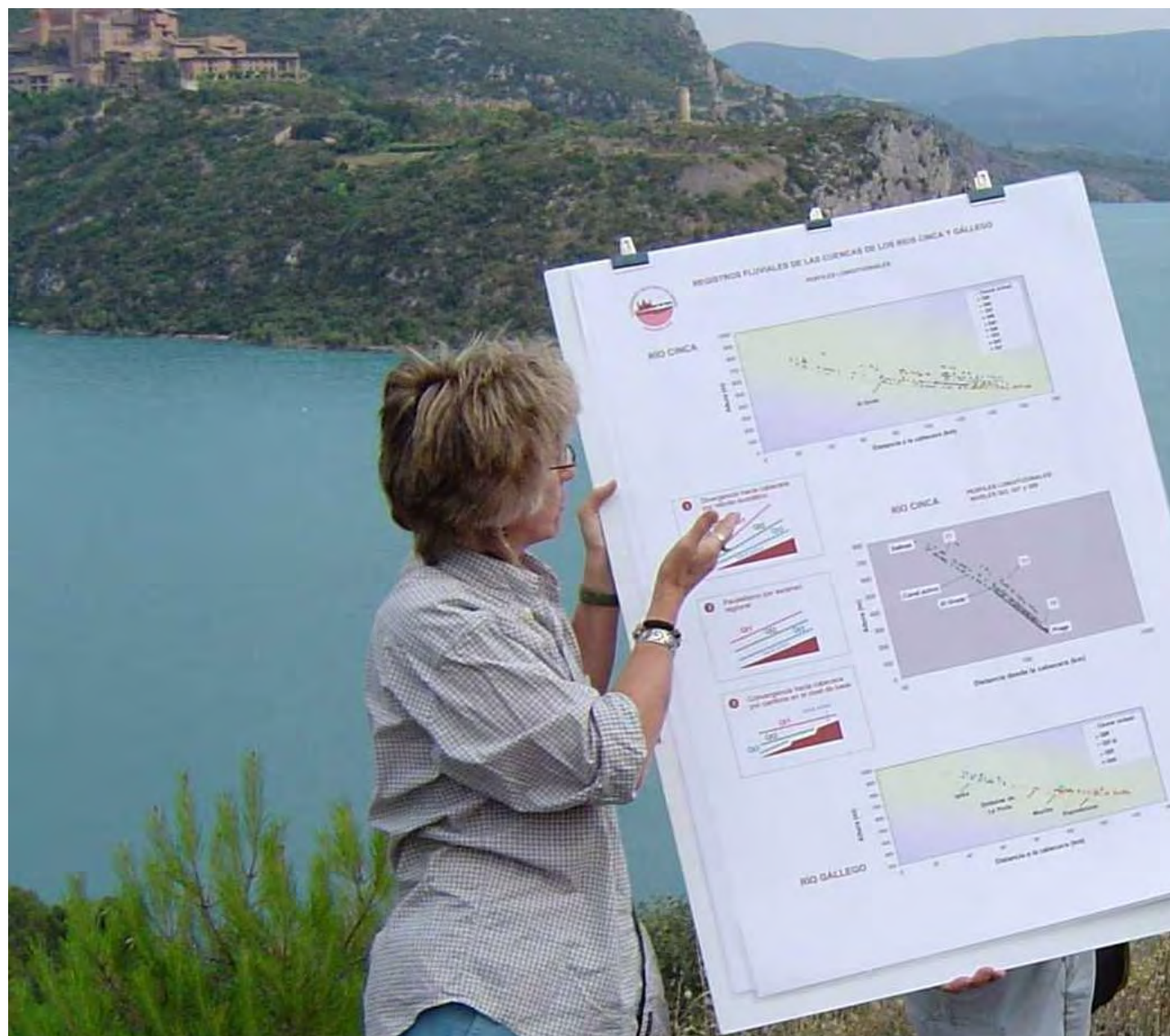


Table 1. Terraces, numerical dates and heights at the Albalate and Ainsa sectors of the Cinca River valley.

Terrace	Age (Ky)	Height (m)	
		Ainsa sector	Albalate sector
<b>Qt1</b>	999-1070 <sup>c</sup>	-	182.1
<b>Qt2</b>	780-999 <sup>c</sup>	-	132.5
<b>Qt3</b>	401±117 <sup>b</sup>	172.5	103.5
<b>Qt4</b>	-	-	91.3
<b>Qt5</b>	178 ± 21 <sup>a</sup>	-	79.9
<b>Qt6</b>	97±16 <sup>a</sup>	-	60.4
<b>Qt7</b>	61 ± 4 <sup>a</sup>	44.2	33.9
<b>Qt8</b>	47 ± 4 <sup>a</sup>	-	13.1
<b>Qt9</b>	11 ± 1 <sup>a</sup>	6.0	3.6

<sup>a</sup> Numerical age from Optical Stimulated Luminiscence (Lewis et al., 2009)

<sup>b</sup> Age derived from soil chronofunction used in Lewis et al. (2009)

<sup>c</sup> Tentative age from paleomagnetic data

Table 2. Summary of relative degrees of soil development on the Cinca River terrace surfaces and estimated ages.

<b>Terrace</b>	<b>PDI Value Range (number of soils)<sup>1</sup></b>	<b>Soil Age<sup>2</sup></b>	<b>Source of Age<sup>3</sup></b>	<b>MAX B Horizon Type<sup>4</sup></b>	<b>MAX Carbonate Stage Morphology<sup>5</sup></b>
<b>Albalate Sector</b>					
<b>Qt9</b>	14.7-18.1 (2)	11±1	OSL	Bk-Bwk	I+
<b>Qt8</b>	23.2-24.7 (2)	47±4	OSL	Bk-Btk	I-II
<b>Qt7</b>	27.0-33.3 (5)	61±4	OSL	Btk-Bkm	II-III
<b>Qt6</b>	43.2 (1)	97±16	OSL	Btk	III+
<b>Qt5</b>	45.1-59.9 (3)	178±21	OSL	Bk-Bkm	III+-IV+
<b>Qt3<sup>6</sup></b>	61.4-80.8 (5)	401±117	PDI	Bt-Bk-Bkm	IV-V+
<b>Ainsa Sector</b>					
<b>Qt9</b>	39.3 (1)	11±1	OSL	Btk	I
<b>Qt7</b>	64.4-67.9 (2)	61±4	OSL	Bt-Btk	I
<b>Qt3</b>	105.1 (1)	-	-	Bt	none

<sup>1</sup> Profile Development Index value and number of soils described shown in ( ). Minimum and maximum PDI values show when more than 2 soils

<sup>2</sup> Age of soil on terrace surface

<sup>3</sup> OSL: Optical Stimulated Luminescence, PDI: age derived from soil chronofunction used in Lewis et al (2009)

<sup>4</sup> Strongest, best develop B horizon type in each soil profiles. Subscripts shown are w: color or structure B; k: accumulation of carbonates; t: accumulation of clay; m: cemented

<sup>5</sup> Carbonate stage morphology from Gile et al. (1981) and Birkeland (1999)

<sup>6</sup> PDI values for the 5 Qt3 soils near Albalate are 61.4, 75.1, 64.9, 64.8, 80.8, respectively

Table 3. OSL dates from terraces in the Cinca River valley (adapted from Lewis et al., 2009).

Lab Code	Terrace	Northing	Easting	De (Gy)	Dose rate (mGy/a)	OSL date (ka)
X398	Qt5	4618380	266866	237±26	1.39±0.09	171± 22
X399	Qt5	4619473	266357	209±7	1.16±0.7	180±12
X397	Qt6	4618085	266253	157±23	1.62±0.11	97±16
X396	Qt7	4700762	265624	156±26	2.46±0.18	63±12
X1122	Qt7	4700762	265624	128±27	2.16±0.12	59±13
X823	Qt7	4678877	270913	82±15	1.28±0.08	64±13
X197	Qt7	4618846	265647	150±3	2.45±0.12	61±3
X199	Qt7	4613809	267775	101±5	1.80±0.09	56±4
X198	Qt7	4613809	267775	118±5	1.82±0.10	65±5
X817	Qt8	4624970	262087	89.0±10.2	2.26±0.14	39±5
X821	Qt8	4614698	267127	83±10	1.96±0.13	42±6
X833	Qt8	4598786	279236	117±6	2.50±0.16	47±4
X808	Qt8	4598765	278848	88±4	1.75±0.10	50±4
X809	Qt8	4598765	278848	90±2	1.79±0.11	50±3
X828	Qt9	270671	270671	18.3±1.1	1.86±0.12	10±1
X826	Qt9	266149	266149	21.8±0.7	1.89±0.13	12±1
X812	Qt9	266149	266149	18.0±7.6	1.46±0.07	9±4
X813	Qt9	266149	266149	27.0±3.6	1.91±0.10	14±2
X816	Qt9	261783	261783	26.5±1.8	2.15±0.14	12±1
X806	Qt9	263612	263612	23.0±2.3	2.03±0.11	11±1
X807	Qt9	263612	263612	22±1.4	1.96±0.10	11±1
X832	Qt9	275009	275009	18.4±3.6	1.81±0.12	10±2



Table 4. Paleomagnetic data. Location and UTM coordinates (T30). n/N; considered/analysed samples. Pol: Polarity. Dec/inc: magnetic declination and inclination and the Fisher (1954) statistical parameters (a95 and K).

Terrace	Pit	X (30T)	Y (30T)	Locality	Samples	n	N	Dec	Inc	a95	K	Pol
<b>Qt7</b>	TA2-1	759286	4700351	Ainsa (Polideportivo)	P85 to P90	3	3	329	32	26.7	33.6	N
	TA4-1	760468	4698252	Banastón (Caballos)	P77 to P84	2	4	13	38	32.0	125.7	N
					<b>PCA only</b>	<b>5</b>	<b>7</b>	<b>346</b>	<b>36</b>	<b>24.0</b>	<b>9.0</b>	<b>N</b>
<b>Qt5</b>	T6-1	766285	4619535	Belver(Plana Valentina)	P01 to P09	6	8	354	64	21.5	12.8	N
	T6-1	765701	4620590	Belver (Granja Baillarín)	P10 to P15	4	5	350	56	54.3	5.1	N
					<b>PCA only</b>	<b>10</b>	<b>13</b>	<b>353</b>	<b>61</b>	<b>19.6</b>	<b>7.9</b>	<b>N</b>
<b>Qt4</b>	T7-1	766023	4622346	Belver (Los Almendros)	P16 & P17	2	4	22	49	37.1	94.8	N
	T7-3	767682	4620960	Belver (Silvio Ballarín)	P44 to P54	3	3	288	55	24.6	10.0	N
					<b>PCA + demagnetization circles</b>	<b>13</b>	<b>13</b>	<b>357</b>	<b>59</b>	<b>12.2</b>	<b>13.6</b>	<b>N</b>
<b>Qt3</b>	T8-1	764028	4628305	Albalate (Los Olivos)	P18 to P24	4	4	26	25	49.7	5.9	N
	T8-2	763799	4627424	Albalate (El Chopo)	blocks P25 to P28	10	11	5	51	12.0	18.9	N
	T8-4	764028	4628305	Albalate (Las Lecineras)	P107 to P110	3	3	339	35	31.3	24.9	N
					<b>PCA only</b>	<b>14</b>	<b>18</b>	<b>357</b>	<b>47</b>	<b>11.0</b>	<b>13.0</b>	<b>N</b>
<b>Qt2</b>	T9-1	765203	4629205	Albalate (Mombrun)	P55 to P57 + P68 to P70	3	3	153	-71	87.3	4.6	R
	T9-2	765126	4628812	Albalate (Mombrun)	P103 to P106	4	4	203	-41	5.7	351.1	R
	T9-3	765200	4628537	Albalate (Mombrun)	P91 to P102	3	3	275	-37	22.9	11.4	R
					<b>PCA + demagnetization circles</b>	<b>9</b>	<b>10</b>	<b>225</b>	<b>-50</b>	<b>18.0</b>	<b>10.3</b>	<b>R</b>
<b>Qt1</b>	T10-2	767495	4629475	Albalate (San Salvador)	P29 to P34	6	7	55	74	44.0	2.9	N
	<b>Cinca Terraces- Reverse</b>					<b>10</b>	<b>10</b>	<b>220</b>	<b>-48</b>	<b>20.6</b>	<b>5.4</b>	<b>R</b>
	<b>Cinca Terraces- Normal</b>					<b>48</b>	<b>58</b>	<b>355</b>	<b>58</b>	<b>10.6</b>	<b>5.7</b>	<b>N</b>
	<b>Cinca Terraces- N+R</b>					<b>58</b>	<b>68</b>	<b>8</b>	<b>57</b>	<b>9.8</b>	<b>5.1</b>	<b>N+R</b>

Table 4. Fluvial incision rates calculated from coupled preserved terraces in the Cinca River valley. Comparison of incision rates at the Ainsa and Albalate sectors is established. Temporal variations of incision rates at the Albalate sector are also evidenced.

Coupled terrace	Differential incision (m)	Elapsed time (Ka)			Incision rate (m/ky)		
		Mean	Minimum	Maximum	Mean	Minimum	Maximum
Qt3-Qt7 Ainsa	128.3	340	219	461	<b>0.38</b>	0.59	0.28
Qt3-Qt7 Albalate	69.6	340	219	461	<b>0.20</b>	0.32	0.15
Qt7-Qt9 Ainsa	38.2	50	45	55	<b>0.76</b>	0.85	0.69
Qt7-Qt9 Albalate	30.3	50	45	55	<b>0.61</b>	0.67	0.55
Qt9-Active channel Ainsa	6.0	11	10	12	<b>0.54</b>	0.6	0.5
Qt9-Active channel Albalate	3.6	11	10	12	<b>0.33</b>	0.36	0.3
Qt1-Qt2 Albalate	49.6	145 <sup>a</sup>	no	no	<b>0.34<sup>a</sup></b>	no	no
Qt2-Qt3 Albalate	29.0	488 <sup>a</sup>	no	no	<b>0.06<sup>a</sup></b>	no	no
Qt3-Qt5 Albalate	23.6	223	85	361	<b>0.11</b>	0.28	0.07
Qt5-Qt6 Albalate	19.5	81	66	108	<b>0.24</b>	0.29	0.18
Qt6-Qt7 Albalate	26.5	36	26	46	<b>0.74</b>	1.02	0.58
Qt7-Qt8 Albalate	20.8	14	22	6	<b>1.48</b>	0.94	3.45
Qt8-Qt9 Albalate	9.5	36	41	31	<b>0.26</b>	0.23	0.31
Qt9-Active channel Albalate	3.6	11	10	12	<b>0.33</b>	0.36	0.30

<sup>a</sup> Indicative data

Y (m)	X (m)	Strath elevation (m)	Substrate	Alluvium thickness (m)	Maximum grain size (Dmax) (cm)	Location	Distance from headwaters (km)
Qt1 strath							
4626238.7	268814.2	357.31	sst, clay	7	48	Monte Julia	130.40
4628762.5	268160.6	369.94	clay, sst	4.5	48	San Salvador	128.00
4631710.0	266994.0	382.77	clay, sst	8.5	43	Brujas	124.70
4633561.1	266598.0	391.65	clay, sst	11	30	Binaced	123.10
					mean = 42 ± 9		
Qt2 strath							
4622779.0	269090.4	291.86	clay	6	40	Belver	138.20
4626128.2	267180.0	307.69	sst	4.5	42	Monte Porquet	134.80
4627915.5	266335.7	316.46	clay, sst	6	48	Mombrun	129.05
4631605.1	265448.4	329.24	clay	5	36	Binaced 2	125.15
4633506.8	265338.9	333.99	clay, sst	6.5	39	Binaced 1	123.35
					mean = 41 ± 4		
Qt3 strath							
4606834.7	275456.5	204.54	clay	2	34	Zaidin south	155.65
4609076.4	274022.9	212.25	clay	3.5	37	Zaidin	153.10
4610459.5	272542.3	221.32	clay	NA	33	San Anton	151.30
4612664.1	272105.5	231.46	ls, clay	4	33	Zaidin north	149.45
4615680.8	270893.7	239.25	clay	2	29	Almudafar	145.45
4617633.2	269497.0	251.03	clay	2	31	Osso	142.79
4624783.7	265615.0	269.81	clay	NA	32	Albalate Porquet	132.10
4625718.6	264849.8	278.70	sst	10	30	Lecineras south	131.25
4627553.2	264705.4	287.57	clay, sst	4.5	38	Lecineras north	129.45
4629600.5	264481.2	299.33	clay	NA	33	Las Brujas west 2	126.85
4630292.1	264604.0	300.16	clay	8.5	33	Las Brujas west 1	126.60
4631856.3	263793.9	302.45	clay	10	46	Alfantega-Albalate	125.15
4633829.1	264075.3	312.84	sl, sst	8.5	33	Alfantega south	123.05
4635456.3	264683.0	324.76	sst, clay	12.5	41	Alfantega north	121.60
4641433.4	267164.4	348.76	sst	2	33	Monzon south	114.30
4642139.0	267230.3	351.28	clay	NA	31	Monzon cemetery	113.60
4643345.2	267354.5	359.67	clay	NA	NA	Monzon castle	112.80
4648994.7	264935.1	384.64	sst clay	3	35	Castejon gravel pit	108.20
4650942.7	264077.2	382.30	gyp	6	NA	Castejon-Salinas	106.10
4651648.2	264273.7	398.07	gyp	5	NA	Castejon	104.70
4652887.4	269341.9	393.82	clay	4.5	26	Fonz 3	104.55
4656953.7	265155.5	427.86	sst, clay	6	26	Las Coronas 3	100.05
4657059.2	265420.3	424.30	clay, sst	6.5	34	Las Coronas 1	99.95
4657890.1	265794.1	427.42	clay, sst	10	35	Las Coronas 4	98.95
4659224.5	266451.3	435.14	cgl, sst	10	NA	Las Coronas 2	97.80

4673397.6	270716.4	507.73	cgl	4	NA	Torreciudad 2	81.55
4673470.8	270762.6	511.44	cgl, clay	NA	NA	Torreciudad	81.55
4674106.1	270586.2	519.12	clay	NA	NA	Torreciudad north	80.90
4679386.0	270652.0	533.57	clay	4.5	35	Abizanda-Moscarazos	75.70
4698766.8	267451.0	687.52	sst, marls	NA	50	Santa Tecla 1	55.80
4698820.7	267324.8	685.63	marls	NA	NA	Santa Tecla 2	55.80
4699527.8	267293.3	698.75	marls, sst	NA	NA	Arnal	54.55
					mean = 34 ± 6		
Qt4 strath							
4618310.2	268999.2	234.51	clay	5.5	41	Osso	142.00
4621360.8	267202.7	249.02	clay	4.5	27	Belver	138.50
4623856.0	265718.1	264.08	clay	6	31	Albalate	134.65
4632761.8	263831.0	299.94	clay, sst	NA	41	Alfaltega south	124.20
4633014.6	263912.7	301.32	cl	NA	43	Binaced road	123.95
4647516.3	264286.8	356.10	clay, sst	NA	26	Castejon 2	109.85
4648272.3	264594.9	360.26	sst, clay, gyp	4	37	Castejon 1	109.05
4648923.5	265099.9	363.73	sst	NA	NA	Castejon gravel pit	108.20
4654312.1	269983.2	397.45	clay	NA	NA	Fonz 1	100.95
4657383.2	270205.3	410.16	clays	NA	NA	Fonz 2	97.95
4671239.3	271297.4	478.68	cgl, sst, clays	6	NA	El Grado	83.90
					mean = 35 ± 8		
Qt5 strath							
4604667.1	276619.5	175.11	clay, sst, lm	3.5	28	Pilaret-Fraga	158.35
4606841.1	275133.3	185.07	clay, marls	3.5	36	Zaidin south	155.45
4608012.4	273923.2	189.64	clay	4	NA	Zaidin	153.85
4612314.6	270700.4	202.56	clay, sst	3	39	Zaidin	148.70
4615106.6	269791.6	219.61	clay	4	51	Almudafar	146.00
4617641.2	268022.3	226.21	clay	5	29	Osso	142.10
4620596.2	266439.1	235.60	clay	5	38	Belver	138.70
4623348.5	264910.9	254.56	clay, sst	5	46	Albalate	134.90
4625398.1	264561.8	257.27	clay	NA	NA	Lecineras	131.50
4627116.2	264081.3	268.53	clay	6.5	37	Clamor	129.90
4629659.3	263752.5	279.92	clay	4	37	Alfantega-Albalate 2	126.75
4631764.0	263530.5	285.61	sst, clay	6	41	Alfantega-Albalate 1	125.30
					mean = 38 ± 7		
Qt6 strath							
4612095.2	270574.9	184.55	clay	6	31	Zaidin	148.80
4614561.5	268279.5	192.57	clay	4	24	Almudafar	145.40
4617395.8	266899.7	205.17	clay	5	38	Osso	141.75
4619988.9	265939.2	215.59	clay, sst	4.5	46	Belver	139.00
4662716.8	271705.9	362.57	sst, marls	NA	30	Estada	98.45
4668560.4	272171.0	416.16	sst	3	27	Artasona	86.45

4710107.9	264958.2	673.64	marls	11	80	Laspuña	43.05
4710475.2	265867.2	683.96	marls	2.5	NA	Laspuña	42.90
					mean = 39 ± 19		
Qt7 strath							
4603962.4	276944.5	136.17	clay, silt	1.5	20	Pilaret	159.15
4608542.3	272710.3	148.99	ls	2	23	Zaidin south	152.80
4609939.6	271780.7	154.18	ls, clays	3.5	25	Zaidin	151.00
4611129.6	270605.8	165.74	clay, ls	1.5	22	Zaidin north	149.60
4612328.1	269279.9	167.12	clay	4.5	22	Almudafar south 1	147.55
4613510.6	268000.6	171.28	clay	4	30	Almudafar south 2	145.95
4613818.8	267774.6	170.83	sst	5.5	24	Almudafar, gravel pit	145.55
4614506.9	267304.1	172.25	sst, clay	4	31	Almudafar north	144.65
4615711.5	266825.8	177.04	ls, clay	2	25	Osso south	143.60
4617975.1	266027.5	188.40	cl	NA	22	Osso north	140.75
4618821.2	265551.1	190.81	sst, ls, clay	4.5	29	Belver Tejerias	139.75
4619145.8	265392.6	189.07	clay	4.5	31	Belver	139.65
4621596.7	264063.9	199.87	sst, silt	NA	28	Albalate 1	136.35
4621619.2	264052.5	199.71	sst, silt	NA	NA	Albalate 2	136.35
4622728.3	263753.3	204.00	silt, sst	2	29	Albalate 3	135.20
4623531.0	263013.5	207.42	clay, sst	3	29	Albalate 4	134.20
4623528.9	259973.4	203.89	silt, clay	4.5	31	Alcolea	133.25
4625094.6	259311.4	209.43	clay	3.5	27	Alcolea north	132.74
4624817.7	262567.7	208.95	clay	7	35	Albalate km 1	132.30
4625514.2	259383.6	209.85	clay	5	NA	Alcolea north 2	131.65
4626568.0	259527.9	213.21	clay	2	25	Santa Lecina	130.70
4626521.5	262161.2	216.06	clay, sst	8	25	Albalate km 3	130.45
4629220.0	260490.3	222.01	sst	2	25	Santa Lecina south	129.60
4628634.8	262493.1	228.18	sst, clay	NA	NA	Albalate km 5.5	128.60
4628801.0	262431.0	226.97	clay	NA	NA	Albalate km 6 a	128.30
4628801.1	262430.8	227.67	clay	6.5	35	Albalate km 6 b	128.30
4630222.5	260538.4	228.20	clay	2	31	Santa Lecina north	126.60
4631295.0	262957.6	235.87	sst, clay	6.5	47	Albalate km 8 a	125.85
4631388.9	263081.3	237.28	sst	NA	37	Albalate km 8 b	125.85
4631924.0	260920.1	234.55	st, clay	NA	NA	Estiche south	125.45
4633048.6	263181.9	241.37	clays	4.5	37	Binaced road	123.95
4633660.7	260901.2	242.52	clay, sst	4.5	39	Estiche	123.80
4634429.6	263302.9	246.29	clay	3.5	37	Alfantega south	122.77
4635076.2	263518.3	248.91	clay	NA	28	Alfantega 1	122.45
4635076.0	263519.1	248.84	clay	NA	NA	Alfantega 2	122.05
4635999.8	261450.7	250.32	clay, sst	3.5	23	Estiche north	121.50
4637344.9	263780.0	258.93	sst, clay	5.5	34	Pueyo 1	119.85
4637984.2	261620.5	261.21	clay	4	22	Pomar north	119.50
4639441.3	264658.1	269.06	sst, clay	NA	NA	Pueyo 2	117.80

4639697.2	262563.3	265.73	clay, sst	NA	NA	Conchel south 1	117.80
4639713.5	262565.1	276.29	clay, sst	3	26	Conchel south 2	117.80
4640762.0	263112.8	269.41	sst, clay	4.5	27	Conchel	116.65
4640326.8	264903.1	270.19	clay, sst	5	32	Alegria	116.55
4641521.3	263719.4	274.05	sst	3.5	28	Conchel north	115.65
4643649.4	264741.5	283.85	sst	2.5	31	Selgua	113.35
4645806.7	265061.4	292.63	clay, sst	3	29	Monzon north	111.25
4647577.6	265271.7	295.37	sst, clay	5	39	Castejon concrete plant	109.55
4647937.3	265274.5	302.00	sst	NA	NA	Castejon a	109.05
4647937.5	265275.1	302.98	sst, clay	NA	40	Castejon b	109.05
4648783.4	266670.7	310.82	not seen	3	30	Chula Vista a	107.95
4648737.8	266624.3	309.66	sst, clay	NA	NA	Chula Vista b	107.95
4648783.4	266670.7	310.82	sst, clay	NA	30	Chula Vista c	107.95
4649518.1	267381.8	307.92	gyp	NA	29	Ariestolas	107.45
4653028.9	268364.0	324.47	clay	4	27	Cofita	104.15
4655141.4	267896.4	338.23	sst	8	39	Fonz	100.80
4657703.6	267937.3	341.73	sst, cgl, clay	5.5	34	Arias II	98.40
4658881.1	268853.8	344.51	cgl	10.5	41	Casa Pararayos	96.50
4659779.8	269184.5	349.60	sst	9	40	Central Electrica Pilas	95.70
4662686.0	269983.7	364.44	clay, sst	12	41	Enate	93.10
4664323.9	270860.5	372.14	clay, sst	9.5	48	Enate north	90.90
4665668.4	271111.9	383.23	cgl, sst	2	33	El Grado south	89.45
4666272.9	271795.1	378.93	sst, cgl	6	32	Olvena	88.90
4667415.4	271756.1	385.12	sst, cgl	9	35	Artasona south	87.60
4669740.5	270777.3	400.65	clay	7.5	42	El Grado	85.35
4670069.9	271665.4	408.35	sst	4	51	El Grado dam 2	85.05
4670299.3	271420.3	402.16	ls	NA	44	Dam	84.75
4678793.0	270908.2	449.57	marl	11	55	Moscarazos	76.05
4684220.2	270139.2	479.93	ls, marls	1.5	33	Liguerre 1	70.50
4685135.5	270156.0	488.43	marls	5	53	Liguerre 2	69.60
4692888.6	268198.3	525.39	marls	NA	NA	Ainsa aerodrome	61.40
4696062.9	267620.1	543.96	marls	3.5	30	Gerbe	58.45
4697188.3	266541.9	550.44	sst, marls	6.5	42	Banaston 1	57.00
4698268.3	266398.0	559.25	marls	8	NA	Banaston 2	55.85
4699552.2	266071.0	566.39	sst	12	NA	Usana	54.55
4700761.5	265623.9	568.12	marls	NA	NA	Pueyo-Ainsa	53.30
4703367.9	265076.6	587.06	marls	10	NA	Ainsa north	50.40
4703968.8	264325.4	599.71	marls	8	NA	Labuerda	49.80
4709582.2	265366.6	650.20	marls	6	NA	Escalona	43.60
4709906.5	265387.2	653.19	marls	2	NA	Escalona2	43.25
4709912.6	265032.2	655.82	marls	5	50	Escuain	43.20
4710744.3	265700.3	662.57	marls	2	40	Laspuña	42.55
4711889.9	265799.1	664.36	marls	3	NA	Laspuña north	41.45

4714062.0	266742.2	697.85	ls	NA	NA	Misuellas	38.90
4713888.6	269696.5	718.61	marls	10	68	Badiain	35.40
					mean = 34 ± 9		
Qt8 strath							
4590370.1	279052.3	80.17	ls	NA	NA	Escarpe, convent a	172.40
4590370.5	279052.6	80.24	ls	NA	NA	Escarpe, convent b	172.40
4590891.4	279123.9	80.10	ls	2.3	25	Masalcorreig a	171.80
4590945.9	279117.4	81.53	ls	NA	NA	Masalcorreig b	171.80
4591745.5	279254.7	86.95	ls	NA	NA	Masalcorreig	171.05
4592329.1	279302.0	8593	marls, ls	4	23	Masalcorreig south	170.35
4593975.4	279633.5	91.86	sst, clay	2.5	27	Masalcorreig north	168.85
4597707.6	279414.7	105.00	clay,sst	2	NA	Fraga south	166.65
4598786.9	279212.5	108.89	clay,sst	3	NA	Fraga hwy	163.95
4599957.9	278910.1	111.15	sst, clay	2	NA	Fraga	162.90
4606658.0	274037.9	125.52	clay, sst, ls	NA	NA	Clamor	154.85
4607369.5	271680.2	137.35	clay	4	28	Velilla south	152.90
4610224.5	268472.5	158.00	clay	2.5	25	Velilla north	148.55
4612890.9	267490.8	145.63	clay	3	31	Almudafar south	146.15
4615161.1	266942.4	158.30	clay, sst	2.5	25	Almudafar north	144.05
4614753.1	265034.6	157.11	clay, marls	2.5	25	Chalamera-Ballobar	143.10
4616088.7	266511.0	166.68	clay	3	NA	Osso	142.65
4617565.5	265856.2	162.10	clay	2.5	35	Osso north	141.15
4617332.9	263643.4	180.52	clay	3	42	Chalamera	140.15
4618685.0	262929.1	179.86	clay	2.5	36	Chalamera north	138.75
4624667.5	262009.9	188.57	not seen	2	22	Albalate	133.90
4651338.4	267816.2	299.06	gyp	NA	28	Cofita south	105.65
4652421.1	267841.3	305.88	gyp, marls	NA	27	Cofita canal	104.65
4660668.2	269984.0	336.43	gyp, marls	NA	NA	Estadilla	94.50
					mean = 29 ± 6		
Qt9 strath							
4596667.0	279164.7	93.79	clay, sst	3	12	Fraga toll rd	160.45
4603299.3	275311.1	101.25	sst, clay	3	28	Miralsot south	152.75
4605605.7	275012.0	116.38	sst, clay	3.5	31	Zaidin south	150.60
4615652.4	265127.9	152.28	clay	2.5	22	Chalamera-Ballobar	136.95
4618197.2	263357.3	159.90	sst, clay	4	28	Chalamera north	133.70
4620341.8	264057.6	168.05	clay	5.5	24	Albalate-Belver	131.85
4623545.6	262027.5	177.68	clay, sst	2	15	Albalate	128.25
4626222.8	261433.0	184.79	sst	2	34	Las Torres	125.50
4627246.1	261894.9	190.18	sst	4	26	Cigüefia	124.50
4632191.0	262278.6	205.64	sst	3	12	Soto del Tros north	119.40
4633967.1	262899.7	213.73	clay, sst	0.5	60	Alfantega	117.55
4636516.8	262991.4	220.84	cl	3.5	26	Pueyo	115.25
4641308.4	264711.2	241.67	sst	3	21	Alegria	110.00

4642910.2	265578.5	244.41	sst	1	NA	Monzon south	108.40
4644355.7	266152.6	251.55	sst, clay	3.5	22	Sosa confluence	106.70
4646366.6	265770.4	263.05	sst	5	21	Monzon north	105.05
4648800.4	266119.5	267.70	sst	NA	NA	Castejon 2	102.45
4648906.0	266183.6	271.11	sst	NA	NA	Castejon 1	102.45
4665046.2	272113.9	341.86	not seen	3	21	Esera confluence	84.35
4667582.6	270679.9	358.33	not seen	NA	NA	El Grado south 1	81.70
4669267.9	270600.1	369.16	not seen	7	37	El Grado south 2	80.40
4686475.7	270644.5	446.97	ls	8	NA	Ligüerre	62.95
4698725.7	265976.7	524.26	marls	3.5	48	Usana	49.60
4710107.5	265784.0	612.75	marls	1	40	Laspuña	37.50
4711924.7	265460.0	627.23	marls	NA	45	Laspuña	35.90
4714416.3	266839.4	657.03	marls	1	38	Hospital de Tella	32.75
4714170.9	269863.3	692.99	ls, marls	2.5	NA	Lafortunada	29.90

mean = 29 ± 12

#### Active channel

4590568.2	278243.3	76.16			NA	Torrente south	167.50
4592675.2	279204.4	74.58			NA	Masalcorreig	164.60
4594870.8	278388.8	79.66			NA	Torrente de Cinca	162.50
4596928.2	278849.5	86.71			NA	Fraga toll rd	160.20
4598806.7	278948.2	91.45			NA	Fraga 1	158.35
4598821.9	278940.5	87.89			NA	Fraga toll rd	158.35
4600248.2	278725.2	94.51			NA	Fraga 2	157.25
4601693.1	278159.6	98.36			NA	Zaidin-Fraga 4	155.95
4603247.8	277358.1	101.14			NA	Zaidin-Fraga 3	154.25
4604209.4	276322.3	106.41			NA	Miralsot south	152.70
4605611.4	274968.5	105.92			NA	Zaidin south gravel pit 2	150.75
4606472.3	274068.0	112.86	ls		NA	Zaidin-Fraga 2	149.55
4608479.0	272650.7	119.77			NA	Zaidin 1	147.05
4609465.8	271366.8	120.59	ls		NA	Zaidin 2	145.70
4610187.2	269704.0	129.27			NA	Ave south	144.05
4610378.3	268514.1	128.03			NA	Ballobar	143.00
4612062.3	267550.6	133.60			NA	Almudafar south	141.15
4613488.6	266644.3	140.72			NA	Almudafar	139.45
4615639.9	265193.2	147.30			NA	Chalamera-Ballobar	137,00
4616710.9	264612.4	148.82			NA	Chalamera	135,55
4618298.0	263415.2	155.20			NA	Chalamera hermitage	133,20
4618566.0	263392.3	160.45			NA	Belver	133,40
4619667.1	263075.0	166.23			NA	Belver north	132.30
4620039.9	262992.4	159.69			NA	Albalate south 1	132.22
4622262.0	262463.6	169.12			NA	Albalate south 2	129.75
4623423.1	261865.3	176.13			NA	Albalate 1	128.30
4623430.2	261865.1	175.24			NA	Albalate 2	128.35



4626195.7	261399.3	180.14	sst	NA	Las Torres	125.50
4627618.6	261822.7	185.31	sst	NA	Ciguena	123.95
4630745.8	261361.0	196.13		NA	Soto del Tros	120.95
4633356.8	261767.0	207.86		NA	Estiche	118.35
4637273.7	262133.7	221.03		NA	Pomar	114.80
4639503.1	262665.8	228.24		NA	Pueyo	112.35
4640927.9	263980.0	235.68		NA	Conchel	110.60
4643437.3	265673.5	241.04		NA	Selgua-Monzon	107.60
4644809.6	265867.9	250.61		NA	Monzon	106.35
4646194.6	265594.6	257.47		NA	Monzon north	105.15
4648060.5	265631.7	258.81		NA	Castejon 1	103.40
4648969.3	266539.5	263.55		NA	Castejon 2	102.20
4650585.0	265670.5	273.82		NA	Castejon 3	101.05
4652004.2	265839.1	277.07		NA	Cofita	99.10
4653915.1	265547.3	285.08		NA	Vero	97.20
4655130.7	266128.3	288.41		NA	Vero north	96.00
4658190.6	266885.9	299.79	sst, cgl dipping 45N	NA	Arias II	92.85
4659504.4	267534.9	306.99		NA	Coronas north	91.50
4660935.1	269750.3	319.45		NA	Puente las Pilas	88.90
4662402.9	270235.1	329.67		NA	Enate 2	87.35
4663979.8	271147.6	336.60		NA	Enate	85.60
4665299.6	271386.7	346.06		NA	Piscifactoria	84.10
4666952.5	271084.7	349.10		NA	Artasona south	82.65
4669068.8	271402.9	358.94		NA	El Grado	80.50
4670028.2	271513.5	365.31		NA	El Grado dam	79.50
4672400.0	271300.0	380		NA		77.15
4677400.0	271000.0	400		NA		72.10
4681300.0	272500.0	420		NA		68.10
4686300.0	274000.0	440		NA		63.05
4889100.0	270000.0	460		NA		60.15
4692750.0	268750.0	480		NA		56.30
4696800.0	266450.0	500		NA		51.55
4699976.5	264920.2	528.59		NA	Ainsa	48.25
4702081.1	264805.0	541.17		NA	Ainsa north	46.05
4704007.1	264807.9	555.85		NA	Labuerda	44.15
4706553.1	265675.7	575.91		NA	Labuerda north	41.35
4710050.0	265753.7	601.17		NA	Laspuña bridge	37.50
4711829.8	265405.3	617.64		NA	Laspuña north	36.00
4711989.0	265561.9	623.30		NA	Puertolas	35.60
4712750.6	266107.4	633.25		NA	Puertolas north	34.80
4713987.4	266833.0	644.17		NA	Misuellas	33.15
4714366.8	268440.4	661.44		NA	Laspuña reservoir	31.40
4715470.8	270601.9	697.83		NA	Devotas	28.05

		740	NA		25.70
4718416.4	270829.7	753.47	NA	Salinas	25.05
		780	NA		23.70
		800	NA		23.45
4720183.9	273539.0	900.84	NA	Bielsa south	21.70
4723000.2	272895.7	973.66	NA	Bielsa	18.65
4724306.0	271381.9	1087.65	NA	Javierre	16.45
4725075.8	268267.4	1161.20	NA	Pineta 2	12.95
4729158.6	261407.7	1273.24	NA	Pineta	5.25
		1300	NA		4.25
		1400	NA		3.75
		1500	NA		3.35
		1600	NA		2.95
		1700	NA		2.75
		2100	NA		2.25
		2200	NA		2.10
		2500	NA		1.25
		2520	NA		0.75
		2600	NA		0.25
		2700	NA		0.03

## Highlights

We used a well-preserved sequence of staircase terraces in NE Iberia to determine spatial and temporal patterns of post-orogenic stream incision.

Mean incision rates since ~400 ka ranged from 0.56 m ka<sup>-1</sup> to 0.38 m ka<sup>-1</sup>.

The combined effects of tectonic and erosional uplift, and climate are discussed.